

**Synthesis and Characterization of Plasma Polymerized  
3,4-Ethylenedioxythiophene Thin Films**

by

Md. Juel Sarder

Roll No: 1018142512

Session: October 2018

MASTER OF SCIENCE IN PHYSICS





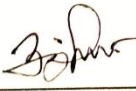
Department of Physics

BANGLADESH UNIVERSITY OF ENGINEERING AND TECHNOLOGY

April, 2022

The thesis titled “Synthesis and Characterization of Plasma Polymerized 3,4-Ethylenedioxythiophene Thin Films” submitted by Md. Juel Sarder, Roll No.: 1018142512F, Session: October-2018, has been accepted as satisfactory in partial fulfillment of the requirement for the degree MASTER OF SCIENCE IN PHYSICS on 23 April, 2022.

### BOARD OF EXAMINERS

1.   
\_\_\_\_\_  
Dr. Mohammad Jellur Rahman (Supervisor)  
Professor  
Department of Physics, BUET, Dhaka. Chairman
2.   
\_\_\_\_\_  
Dr. Nasreen Akter  
Professor and Head  
Department of Physics, BUET, Dhaka. Member  
(Ex-officio)
3.   
\_\_\_\_\_  
Dr. Md. Forhad Mina  
Professor  
Department of Physics, BUET, Dhaka. Member
4.   
\_\_\_\_\_  
Dr. Muhammad Rakibul Islam  
Associate Professor  
Department of Physics, BUET, Dhaka. Member
5.   
\_\_\_\_\_  
Dr. A. B. M. Obaidul Islam  
Professor  
Department of Physics, University of Dhaka,  
Dhaka. Member  
(External)

## CANDIDATE'S DECLARATION

It is hereby announced that this article or any part of it has not been submitted elsewhere for the award of any degree or diploma.



---

Md. Juel Sarder

**DEDICATED  
TO  
MY BELOVED PARENTS**

## Acknowledgements

At the very beginning, all praise and endless gratitude to my great creator Allah Who has given me the patience, strength and knowledge that enabled me to complete this research work.

My heartfelt gratitude and generosity to Dr. Mohammad Jellur Rahman, Professor, Department of Physics, Bangladesh University of Engineering and Technology (BUET), for his unwavering support and outstanding guidance throughout my research work, encouraging creative ideas, critical thinking, and inspiration. I express my heartfelt thanks to Prof. Dr. Nasreen Akter, Head of the Department of Physics at BUET, Dhaka, for providing necessary facilities, precious suggestions and supports to conduct my research study.

I am overjoyed to be able to offer my heartfelt appreciation to Prof. Dr. Md. Feroz Alam Khan, Prof. Dr. Jiban Podder, Prof. Dr. A. K. M. Akther Hossain, Prof. Dr. Md. Forhad Mina, Prof. Dr. Md. Rafi Uddin, and Prof. Dr. Mohammed Abdul Basith, Department of Physics, BUET, for their helpful suggestions and assistance. I would want to convey my gratitude to Dr. Muhammad Rakibul Islam, Dr. Parvin Sultana, Dr. Mehnaz Sharmin as well as all the faculty members of the Department of Physics, BUET for a slew of ideas and inspirations. I appreciate the authority as well of Committee for Advanced Studies and Research (CASR), BUET for the financial support for this thesis work.

I extend my deepest gratitude to Mr. Md. Mahmud Hasan, Mr. Md. Johurul Islam, Mrs. Rani Nasrin, Miss. Farzana Yasmin, Mr. Md. Saddam, and Mr. Md. Mehdi Hasan Shohag for giving me encouragement and warm support. I am so grateful to the Ministry of Science and Technology for providing me National Science and Technology (NST) fellowship. I would like to express my gratitude to the Nanotechnology Research Laboratory, Department of Physics, BUET for providing me experimental data using their devices of UV-visible spectroscopy.

Furthermore, I want to express my gratitude to my parents, brothers, sisters, and other family members for their unwavering love, devotion, encouragement, care, and invaluable support shown to me throughout the years.

## Abstract

Plasma polymerized 3,4-ethylenedioxythiophene (PPEDOT) thin films have been deposited onto glass substrates at room temperature under AC (50 Hz) and RF (13.56 MHz) power sources by using the plasma polymerization (PP) technique. 3,4-ethylenedioxythiophene (EDOT) has been chosen as a monomer precursor. The thicknesses of the films measured by Multiple-Beam Interferometer have varied with increasing deposition times. The field emission scanning electron microscopy (FESEM) images exhibit that the surface morphology of the films is immaculate and pinhole-free. The Fourier transform infrared spectroscopy analysis represented that the chemical compositions as deposited PPEDOT films are different from that of the EDOT monomer, indicating some structural rearrangement. The energy band gap values of the PPEDOT (AC) thin films decrease from 3.75 to 3.54 eV with the increase of film thickness. The Urbach energy, steepness parameter, extinction coefficient, refractive index, and other optical parameters are studied to indicate suitability of these films for use in various electrical and optoelectronic devices. Both TG and DSC reveal that these films are thermally stable up to 612 K temperature. DC electrical analysis exhibits that space charge limited conduction (SCLC) mechanism is active in the PPEDOT (AC) thin films. The activation energy,  $\Delta E$ , values of the PPEDOT (AC) thin films in the Ohmic region are found to be around 0.076 eV whereas, in the non-Ohmic region,  $\Delta E$  values are found to be around 0.119 eV. A comparative study has also been done on the PPEDOT thin films deposited using RF (13.56 MHz) power and observed that RF power source can produce thicker films within shorter time compared to AC power source, but no significant changes are found in the film's quality in terms of structural, optical, and electrical properties.

## CONTENTS

	<b>Page No.</b>
Candidate's Declaration	iii
Dedication	iv
Acknowledgements	v
Abstract	vi
Contents	vii
List of Figures	x
List of Tables	xiv
List of Abbreviations	xvi
<b>CHAPTER 1</b>	<b>INTRODUCTION</b>
	<b>(1-5)</b>
1.1 Organic Thin Films	1
1.2 Objectives	3
1.3 Outline of the Thesis	4
<b>CHAPTER 2</b>	<b>LITURATURE REVIEW AND THEORITICAL</b>
	<b>ASPECTS</b>
	<b>(5-15)</b>
2.1 Brief Reviews on Plasma Polymerized (PP) Thin Films	5
2.2 Theory of Plasma Polymerization	12
2.2.1 Advantages in this process	14
2.2.2 Applications of PP thin films	14
<b>CHAPTER 3</b>	<b>MATERIALS AND METHOD</b>
	<b>(16-24)</b>
3.1 Monomer	16
3.2 Substrate and its Cleaning	16
3.3 PP Set-up and Deposition Process	17
3.4 Thickness Measurement	20
3.5 Electroding Process	21
3.6 Characterization Techniques	22

3.6.1	Field emission scanning electron microscopy (FESEM) and energy dispersive x-ray (EDX)	22
3.6.2	Fourier transform infrared spectroscopy and relevant theories	22
3.6.3	UV-visible spectroscopy and relevant theories	23
3.6.4	Differential thermal and thermo-gravimetric analysis	23
3.6.5	DC electrical measurement and relevant theories	23
<b>CHAPTER 4 RESULTS AND DISCUSSION</b>		<b>(25-57)</b>
4.1	Surface Morphology and Compositional Analyses	25
4.1.1	FESEM study	25
4.1.2	EDX analyses	27
4.2	Structural Analyses by FTIR Spectroscopy	28
4.3	UV-Visible Spectroscopic Analyses	30
4.4	Thermal Analysis: TG/DSC of AC PPEDOT films	38
4.5	DC Electrical Properties of PPEDOT (AC) Thin Films	40
4.5.1	Current density-voltage ( <i>J-V</i> ) characteristics	40
4.5.2	Dependence of <i>J</i> on temperature	43
4.6	Morphological, Structural, Optical, Thermal, and DC Electrical Properties of PPEDOT (AC) Thin Films with Previous Works.	44
4.7	Comparative Study Among Various Characteristics of AC and RF PPEDOT Thin Films	45
4.7.1	FESEM study	45
4.7.2	EDX analyses	47
4.7.3	Structural analyses by FTIR spectroscopy	48
4.7.4	UV-Vis spectroscopic analyses	49
4.7.5	TG/DSC of RF PPEDOT films	53
4.7.6	DC electrical properties: <i>J-V</i> characteristics	54
4.7.7	Dependence of <i>J</i> on temperature	56
<b>CHAPTER 5 CONCLUSIONS</b>		<b>(58-59)</b>
5.1	Summary	58
5.2	Conclusions	60



5.3	Scope of Further Research
	References

61
(62-67)

## List of Figures

<b>Fig. No.</b>		<b>Page No.</b>
Fig. 2.1	FESEM micrograph of the (a) PhmEDOT and (b) PEDOT thin films.	6
Fig. 2.2	(a) FESEM images of the as-deposited PPPA thin film, (b) The FTIR spectra for monomer PA and PPPA as-deposited.	6
Fig. 2.3	The FTIR spectra as deposited of PEDOT thin films.	7
Fig. 2.4	(a) Transmittance spectra of PEDOT: PSS thin films, (b) current density-voltage curves of PEDOT: PSS thin films.	8
Fig. 2.5	(a) Absorbance spectrum to wavelength of NCC, PEDOT, and NCC/PEDOT thin film, (b) bandgap energy of PEDOT thin films.	9
Fig. 2.6	EDX spectra of the PPNBA thin films of different thicknesses.	9
Fig. 2.7	(a) $J$ - $V$ for PPBMI thin films of various thicknesses at room temperature, (b) variation of $J$ versus $V$ at various temperatures for PPBMI thin film (thickness, $d = 200$ nm).	10
Fig. 2.8	(a) Absorption coefficient and (b) extinction coefficient $k$ as a function of the wavelength for different RF power.	11
Fig. 2.9	TGA thermographs as deposited PPCHex in oxygen environment (scan rate 10 K/min).	11
Fig. 2.10	(a) DSC and, (b) TGA curves of the PEDOT: PSS, GO 0.05, 0.15, 0.25 PEDOT films.	12
Fig. 2.11	(a) A schematic PP configuration and (b) schematic comparison of the structures of plasma polymers and conventional polymers.	12
Fig. 2.12	The schematic overview of the basic processes in a glow discharge.	13
Fig. 3.1	The chemical structure of EDOT and PEDOT.	16
Fig. 3.2	Schematic diagram of the plasma polymerization set up in laboratory.	18
Fig. 3.3	Glow discharge plasma: (a) before deposition (b) during deposition, and (c) prepared PPEDOT samples.	19

Fig. 3.4	Diagram of Fizeau interferometer used for the measurement of thin film thickness (Inset: Fizeau fringe pattern of the PPEDOT thin films).	20
Fig. 3.5	Electrode assembly: (a) Lower electrode, (b) lower electrode and the sample, (c) sample in between the upper and lower electrode.	21
Fig. 4.1	FESEM micrographs of the PPEDOT (AC) thin films at different magnifications of thickness 330 nm, (a) $\times 30$ k, (b) $\times 50$ k, (c) $\times 100$ k.	26
Fig. 4.2	(a), (b), (c) FESEM micrographs of the PPEDOT thin films at thicknesses of 240 nm, 330 nm, and 390 nm at magnification of $\times 50$ k, respectively.	26
Fig. 4.3	(a), (b) and (c) Represent EDX spectra of the PPEDOT thin films of thicknesses 250 nm, 330 nm, 390 nm, respectively.	27
Fig. 4.4	FTIR spectra of EDOT monomer; as-deposited PPEDOT (AC) thin films at various thicknesses.	29
Fig. 4.5	Spectral distribution of absorbance of PPEDOT (AC) films as a function of wavelength.	31
Fig. 4.6	Spectral distribution of transmittance of PPEDOT (AC) films.	31
Fig. 4.7	Plot of absorption coefficient, $\alpha$ with $h\nu$ , for as-deposited PPEDOT thin films of different thicknesses.	32
Fig. 4.8	Band gap energy of PPEDOT thin films using the Tauc relation of different thicknesses.	33
Fig. 4.9	The $\ln \alpha$ vs $h\nu$ plots for thickness dependent PPEDOT (AC) films.	34
Fig. 4.10	The variation of extinction coefficient, $k$ with $\lambda$ for as-deposited PPEDOT (AC) films.	35
Fig. 4.11	The refractive index plots against $\lambda$ for as-deposited PPEDOT (AC) thin films.	36
Fig. 4.12	The optical conductivity ( $\sigma_{opt}$ ) with wavelength of thickness dependent PPEDOT (AC) films.	37
Fig. 4.13	The variation of skin depth ( $\chi$ ) against photon energy for the	37

as-deposited thickness dependent PPEDOT (AC) films

- Fig. 4.14 Thermograms of (a) TGA; (b) DSC of thickness dependent PPEDOT thin films in N<sub>2</sub> environment at scanning rate of 10 K/min. 39
- Fig. 4.15  $J$ - $V$  relationship for PPEDOT (AC) films of thickness (a) 250 nm, (b) 330 nm and (c) 390 nm at different temperatures, (d) for the film at room temperature (298 K). 41
- Fig. 4.16 Plots of  $J$  vs  $d$  for PPEDOT (AC) thin films in the non-Ohmic region (at voltage 60 V). 43
- Fig. 4.17 Variation of  $J$  with  $1/T$  for PPEDOT (AC) thin films of thicknesses 250 nm, 330 nm, and 390 nm at (a) 10 V (Ohmic) and (b) 60 V (non-Ohmic) regions. 44
- Fig. 4.18 Comparison of FESEM surface morphology images as deposited (a)  $\times 50$  k, (c)  $\times 100$  k for PPEDOT (AC), and (b)  $\times 50$  k, (d)  $\times 100$  k for PPEDOT (RF) films. 46
- Fig. 4.19 Cross-sectional view PPEDOT (RF) of thickness 690 nm. 46
- Fig. 4.20 EDX spectra of (a) AC (37 W) and, (b) RF (37 W) of PPEDOT thin films. 47
- Fig. 4.21 FTIR spectra as-deposited AC (37 W) and RF (37 W) PPEDOT thin films. 48
- Fig. 4.22 (a) Spectral distribution of (a) absorbance, (b) transmittance of AC (37 W) and RF (37 W) PPEDOT films as a function of wavelength. 50
- Fig. 4.23 (a) Plot of absorption coefficient,  $\alpha$  with  $h\nu$ , (b) band gap energy using the Tauc relation, for PPEDOT thin films of different plasma power. 50
- Fig. 4.24 (a) The  $\ln\alpha$  vs  $h\nu$  plots, (b) extinction coefficient,  $k$  with  $\lambda$ , for AC and RF PPEDOT thin films. 51
- Fig. 4.25 (a) The refractive index plot against  $\lambda$ , (b) the optical conductivity ( $\sigma_{opt}$ ) with wavelength and, (c) the skin depth ( $\chi$ ) against photon energy, for AC and RF PPEDOT thin films. 52

- Fig. 4.26 (a) Weight loss and (b) DSC of PPEDOT thin films in nitrogen atmosphere at scanning rate of 10 K/min. 53
- Fig. 4.27 Current density ( $J$ ) - Voltage ( $V$ ) relationship at different temperatures for (a) PPEDOT (AC) and (b) PPEDOT (RF) films deposit at same power (37 W). 55
- Fig. 4.28 Comparison of  $J$  on  $I/T$  for PPEDOT (AC) and, PPEDOT (RF) thin films at (a) 10 V (Ohmic) and (b) 60 V (non-Ohmic) regions. 56

## List of Tables

Table No.		Page No.
Table 2.1	Elemental composition of V <sub>2</sub> O <sub>5</sub> , V <sub>2</sub> O <sub>5</sub> -PEDOT, MoO <sub>3</sub> thin films on ITO coated PET film.	7
Table 3.1	General properties of 3,4-ethylenedioxythiophene.	17
Table 3.2	Optimized conditions for thin film deposition	19
Table 4.1	Atomic percentage (at%) of the elements present in the PPEDOT thin films.	28
Table 4.2	The FTIR spectroscopic assignments of the EDOT monomer and PPEDOT (AC) thin films.	29
Table 4.3	Bandgap and $\lambda_{max}$ values of PPEDOT thin films of different thicknesses.	33
Table 4.4	Variation of $E_u$ and $\sigma_s$ of as-deposited PPEDOT thin films.	35
Table 4.5	The weight loss (wt%) and stability temperature of PPEDOT (AC) thin films.	40
Table 4.6	The slopes in the lower (<10 V) and higher voltage (>10 V) regions at different temperatures for PPEDOT (AC) thin films.	42
Table 4.7	Activation energy, $\Delta E$ (eV) for PPEDOT (AC) thin films of several thicknesses.	44
Table 4.8	Various properties of PPEDOT (AC) thin films and previous work.	45
Table 4.9	Atomic percentage (at%) of the elemental distribution in the PPEDOT thin films.	47
Table 4.10	The FTIR spectroscopic assignments of the AC and RF PPEDOT thin films.	49
Table 4.11	Bandgap and $\lambda_{max}$ values of PPEDOT thin films of different thicknesses.	51
Table 4.12	Variation of $E_u$ and $\sigma_s$ of as-deposited PPEDOT thin films with film thicknesses.	51
Table 4.13	The weight loss (wt%) and stability temperature of AC and RF PPEDOT thin films.	54

Table 4.14	The slopes in the lower and higher voltage regions at different temperature for PPEDOT thin films of different power sources.	55
Table 4.15	Values of activation energy $\Delta E$ (eV) for PPEDOT (AC) and PPEDOT (RF) thin films.	56
Table 4.16	Morphological, structural, thermal, optical and DC electrical properties of AC and RF PPEDOT thin films.	57

## List of Abbreviations

<b>AC</b>	Alternating Current
<b>DC</b>	Direct Current
$\lambda$	Wavelength
<b>Al</b>	Aluminum
<b>RF</b>	Radio Frequency
<b>DTA</b>	Differential Thermal Analysis
<b>DSC</b>	Differential Scanning Calorimetry
<b>DTG</b>	Differential Thermograph
<b>FTIR</b>	Fourier Transform Infrared
<b>FESEM</b>	Field Emission Scanning Electron Microscopy
<b>EDX</b>	Energy Dispersive X-ray
<b>UV-Vis</b>	Ultraviolet-Visible
$k_B$	Boltzmann Constant
$k$	Extinction Coefficient
<b>PECVD</b>	Plasma Enhanced Chemical Vapor Deposition
$A$	Absorbance
$T$	Transmittance
$\alpha$	Absorption Coefficient
$E_{g(d)}$	Direct Band Gap
$E_{g(i)}$	Indirect Band Gap
$E_u$	Urbach Energy
$\sigma_s$	Steepness Parameter
$\mu$	Refractive Index
$n$	Power Index
$\epsilon_0$	Permittivity of Free Space
$J$	Current Density
$\Delta E$	Activation Energy
$\nu$	Frequency
$H$	Planck Constant
$D$	Thickness



# CHAPTER 1

## INTRODUCTION

### 1.1 Organic Thin Films

With the advancement of modern technology and the growth of the global economy, the demand for polymer thin films with a variety of applications has increased significantly, because of their tiny weight and interesting physio-chemical properties [1].

A thin film is a coating of material that is exceedingly thin, ranging in thickness from fractions of a nanometer to several micrometers. A thin film consists of a two-dimensional thin layer of material created atom by atom or molecule by molecule in the scientific sense. Thin films have been used as protective coatings from the beginning of time. The extraordinary expansion of thin film development in the fields of optoelectronic devices, manufacturing technologies, novel materials development, and other fields, Physics is producing a new branch known as thin film technology. Thin-film technology has advanced tremendously in recent decades because of the industry demand for successful thin-film microelectronic products. Organic polymer thin films have attained significant research attention because of their potential in modern technologies such as in diodes, transistors [2], gas and humidity sensors [3-5], implants [6], optical waveguides [7], micro-electronic devices [8], nonlinear optical and molecular devices [9]. Moreover, organic semiconductor-based device technology is less expensive and easier to construct than inorganic devices.

There have a lot of deposition techniques reported for thin films, such as spin or spray coating, solution-based techniques [10, 11], electrochemical deposition [12], plasma enhanced chemical vapor deposition (PECVD) [13], oxidative type in-situ polymerizations [14], and atmospheric plasma deposition [15] on to solid substrates. Among these, plasma polymerization (PP) technique, one form of PECVD, has become an important method for preparing organic thin films. The PP method has good deposition aspects such as faster deposition rate, uniformity, thickness control, and mechanical stability [16]. Again, it becomes a cheaper method and environment friendly [17]. It can develop high cross-linked thin films, which can supply chemical

characteristics [18] and is recognized as a direct film deposition method of entirely new kinds of polymeric thin films [11]. The PP technique generates materials which are significantly different from conventional polymers and most inorganic compounds. Conventional polymerization techniques need to contain functional groups of monomers during deposition, but PP is the direct polymeric deposition method where each type of organic monomer can be deposited without toxic solvents [16]. This plasma polymerized organic thin films are now attracting research attention due to their relative ease of synthesis, chemical and mechanical stability, high surface functionalization, and unique optoelectronic properties [19]. As a result, the PP technique should be conceived of as a new attractive technique for creating unique materials rather than manufacturing existing polymers.

Different recent studies have explored the optical, morphological, and electrical properties of PP thin films, because the exact information of the PP thin films is reliant on many variables such as discharge power, precursor structure, substrate temperature, monomer flow rate, and so on [26], and therefore those properties can be tuned by changing any of the parameters. As a result, several research on thin polymeric films have been conducted, but these materials still require more investigation to develop high-quality and sophisticated materials for electrical, electronic, and optical devices in industrial and scientific applications.

In this study, a highly conducting monomer, 3,4-ethylenedioxythiophene (EDOT) has been chosen as a monomer precursor to deposit plasma polymerized EDOT (PPEDOT) thin films using both AC (50 Hz) and RF (13.56 MHz) plasma. So far, only a few reports are found in the literature about poly 3,4-ethylenedioxythiophene (PEDOT) thin films and their deposition techniques are also different from ours. Again, no study has yet been found in the literature which reports the thermal and electrical properties of the PEDOT thin films. PEDOT has some interesting physio-chemical properties such as lower optical band gap, higher electrical conductivity and thermal stability etc. This material is an optically transparent and highly air-stable conductive polymers among the most promising candidates in this field and has advantages over their inorganic counterpart [21]. As a highly conducting polymer, EDOT has a new perspective for recent applications in organic photovoltaic (PV) technology and proved to be advanced material [22] because of its high optical transparency, extremely good chemical

stability, and redox potential in the doped states [23, 24]. PEDOT films are deposited as one of the layers of organic solar cells, where mostly spin coating method is used. But, the efficiency of this type of solar cells haven't signified the commercial solar panels efficiency till now. Changing deposition technique or other parameters would be an interesting field of research with the aim to increasing the efficiency of this type of solar cells. That's why PPEDOT thin films have been deposited using PP method and different properties of the PPEDOT thin films such as morphological, structural, optical, thermal, and electrical properties are investigated.

The type of power sources like DC, AC, RF, pulsed, and magnetron-assisted plasmas are used in the PP process. Though, AC power source is widely used in PP technique but recently, radio frequency (RF) power source has been used as an alternative power of AC to generate glow discharge plasma for obtaining unique kinds of cross-linked polymeric compounds as uniform, homogenous and amorphous thin films [6, 20]. It increases the absorption peak intensities of thin films that indicates higher quality film deposition [21]. So, in this research, a comparative study on different properties of the PPEDOT thin films deposited using AC and RF has also been reported to find out which can produce films of better quality.

## 1.2 Objectives

The main objectives of this research are as follows:

- Synthesis of PPEDOT thin films using capacitively coupled glow discharge plasma and study of their surface morphology using field emission scanning electron microscopy (FESEM) and elemental composition using energy dispersive X-ray (EDX) analysis.
- To identify the functional groups of PPEDOT thin films via Fourier transform infrared (FTIR) spectroscopy and analyze thermal stability of the PPEDOT thin films.
- Investigation of optical and electrical properties of the PPEDOT thin films of different thicknesses at different temperatures.
- Comparison of different properties of the films produced by AC and RF systems to find their suitable applications in electrical and optoelectronic devices.

### 1.3 Outline of the Thesis

**Chapter One** contains a brief overview of the research background and purpose, as well as the current state of the topic.

In **Chapter Two**, a summary of the different studies on organic thin film utilized in this study are presented. The technique for their synthesis, significant physical features, and a literature study in pertinent fields are presented. For a better understanding of this research, a brief review of PPEDOT thin films and its characterizations are also presented.

In **Chapter Three**, the experimental details are described. It covers AC/RF PP process of thin film preparation, the description of the capacitively coupled glow discharge system, and thin film thickness measurement technique used. This chapter goes through the techniques used to characterize thin films, such as FESEM, FTIR, UV-visible spectroscopy, TG/DSC, and DC electrical measurements.

**Chapter Four** offers detailed investigations of morphological, elemental, structural, optical, thermal, and current voltage characterization of PP thin films. The mechanism of charge transfer in thin the films are also explored.

Finally, in **Chapter Five**, the summary of the study and conclusions with future scope of the investigation are presented.

## CHAPTER 2

### LITURATURE REVIEW AND THEORITICAL ASPECTS

#### 2.1 Brief Reviews on Plasma Polymerized Thin Films

Glow discharges are widely being used for the polymerization of a variety of organic and organometallic compounds. Since the 1960s, plasma polymerization (also known as glow discharge polymerization) has been identified as a method of manufacturing polymers by forming unwanted by-products in plasma [25]. Organic thin films have lately become quite famous due to their rapid growth and widespread use. However, it was known for many years in the early stages that some organic compounds created solid deposits in plasma-generated electrical discharges. Most onlookers assumed the deposits were merely by-products. Naturally, these undesired by-products received some attention, either for their qualities or for their potential to be used in the production of extremely useful materials.

Because of the unique structure resulting from the formation mechanism, PP organic thin films exhibit remarkable optical and electrical characteristics that are ideal for a variety of devices. Over the years, scientists have focused their studies on PP organic and organometallic thin films to develop novel materials with promising features for current science and technology applications. Here is a quick rundown of the studies:

Lin *et al.* [26] studied the electrochromic properties of poly (hydroxymethyl 3,4-ethylenedioxythiophene) (PhmEDOT) and PEDOT thin films. Indium tin oxide conducting glass was used to prepare these thin films by electro-polymerization method. A three-dimensional network-like structure SEM images have been obtained by this method as shown in Fig. 2.1. It was observed that the PhmEDOT thin film has higher film porosity compared to the PEDOT thin film. The presence of hydroxymethyl functional groups may induce intermolecular or intramolecular interactions, possibly the H bonding, and a more porous film structure was therefore derived.

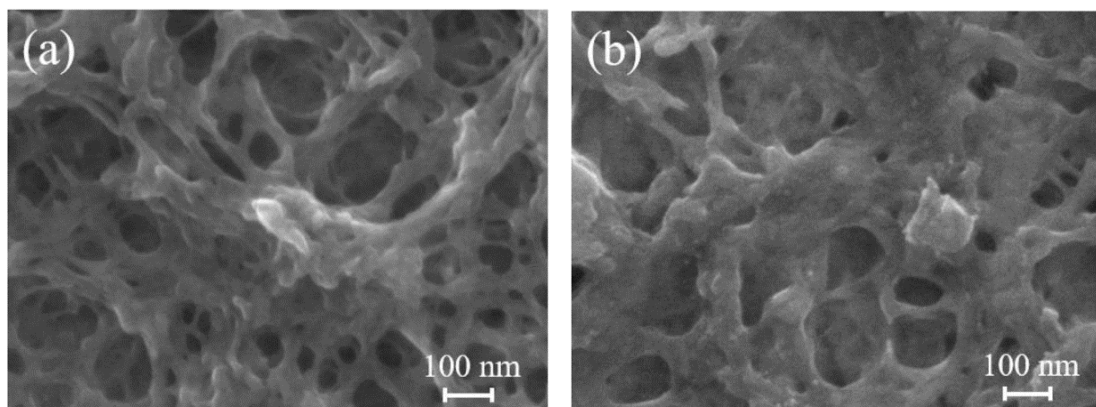


**Fig. 2.1** FESEM micrograph of the (a) PhmEDOT and (b) PEDOT thin films. [26].

Kabir *et al.* [27] studied surface morphology of PP pyromucic aldehyde (PPPA) thin films as shown in Fig. 2.2 (a). They also were investigated the structural and optical aspects of the thin films. As can be seen from the micrographs, the surface of the PP thin films is uniform, perfect, pinhole-free, and fracture-free. They also repeated that the FTIR spectra of pyromucic aldehyde (PA) and as-deposited PPPA (curves P and Q, respectively) demonstrated structural alterations caused by plasma polymerization of the monomer PA as shown in Fig. 2.2 (b).

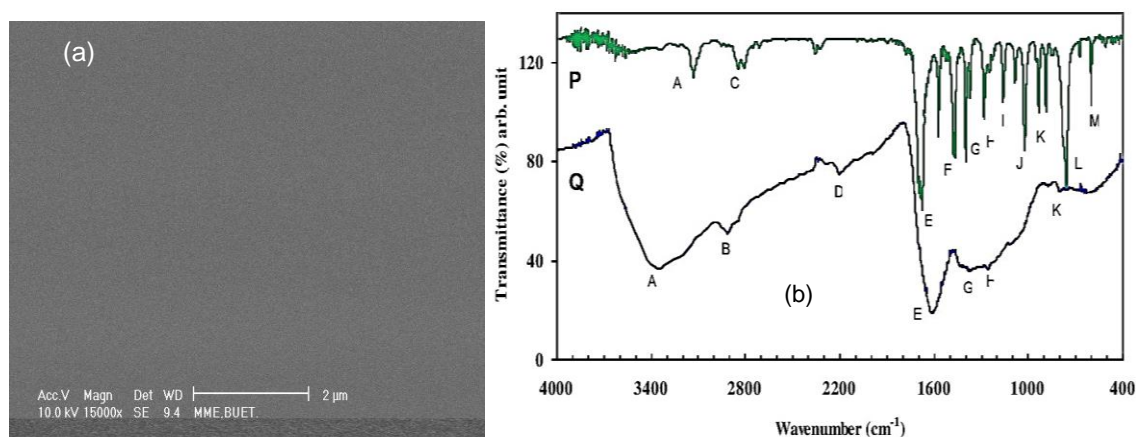


**Fig. 2.2** (a) FESEM images of the as-deposited PPPA thin film, (b) the FTIR spectra for monomer PA and PPPA as-deposited. [27].

Karaca *et al.* [28] studied the plasma modified Vanadium oxide/poly (3,4-ethylenedioxythiophene) ( $V_2O_5$ -PEDOT) hybrid based flexible electrochromic devices in which hybrid materials were prepared in a rotating quartz plasma reactor via capacitively coupled RF (13.56 MHz) plasma. Smooth surface of the films without any fragmentation have been prepared using the SEM and energy dispersive X-ray (EDX)

spectroscopy analyses. The EDX results of  $V_2O_5$ ,  $V_2O_5$ -PEDOT hybrid and  $MoO_3$  thin films are noted in Table 2.1. The elemental composition of  $V_2O_5$ -PEDOT film including additional carbon and sulfur elements with, decreasing oxygen and vanadium elements confirmed the presence of PEDOT on spherical particles of  $V_2O_5$ . In  $MoO_3$  on ITO coated polyethylene terephthalate film, the atomic content of molybdenum, oxygen (%) were observed as 10, 90, respectively.

**Table 2.1** Elemental composition of  $V_2O_5$ ,  $V_2O_5$ - PEDOT,  $MoO_3$  thin films on ITO coated PET film.

Samples	at. % Ratio				
	Carbon	Oxygen	Sulfur	Vanadium	Molybdenum
$V_2O_5$ (untreated)	-	98.6	-	1.4	-
$V_2O_5$ - PEDOT	52	46	0.93	1.07	-
$MoO_3$	-	90	-	-	10

Kiristi et al. [29] analyzed structural formation of PEDOT and noted some significant bands using RF PP method. They have specified that randomly deposited cross-linked structures took place in the polymeric thin film and this formation causes weaker signals in the FTIR spectra as shown in Fig. 2.3. The plasma processes affected the position and the number of peaks which confirmed by FTIR spectra analysis.

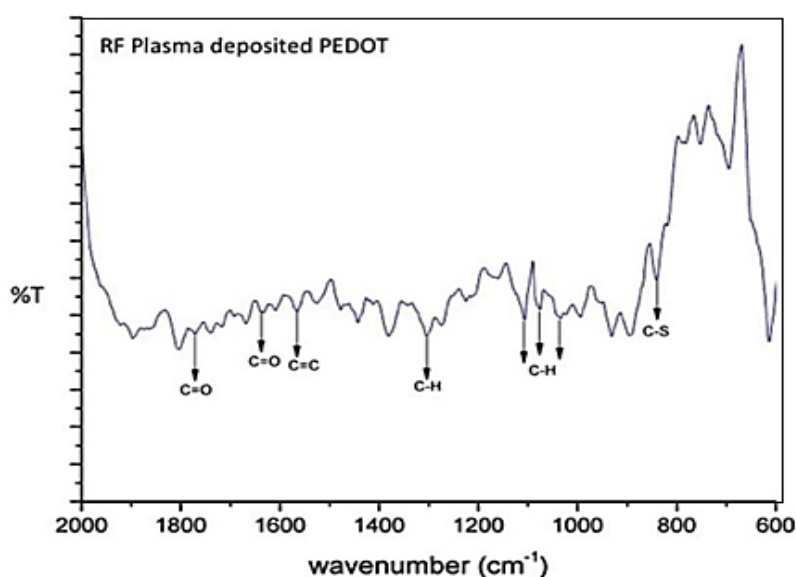


**Fig. 2.3** The FTIR spectra as deposited of PEDOT thin films [29].

Chang *et al.* [30] studied the enhanced electrical conductivity of PEDOT: PSS thin films for ITO-free organic photovoltaics and presented the optical and mechanical properties of highly conductive PEDOT: PSS (1:2.5 wt%, PH1000) thin films. These films were made using a solution comprising 67% ethylene glycol and 33% hexafluoro-isopropyl alcohol by volume, without utilizing an immersion treatment method. As demonstrated in Fig. 2.4 (a), the average transmittance of the PEDOT: PSS thin films was more than 85% in the visible range. When the unmodified PEDOT: PSS thin film was utilized as the anode electrode, the device performances detached PEDOTs resulted in a modest, short-circuit current density and fill factor, according to the  $J$ - $V$  curve analysis illustrated in Fig. 2.4 (b). Because of the greater resistance, they determined that PEDOT: PSS thin film had a poor electrical conductivity (0.84 S/cm).

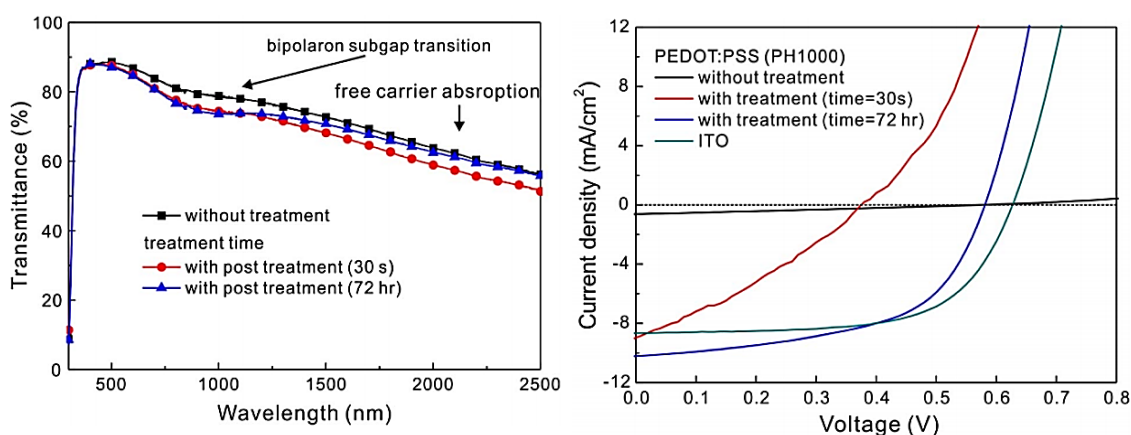


**Fig. 2.4** (a) Transmittance spectra, (b) current density-voltage curves of PEDOT: PSS thin films [30].

Ramdzan *et al.* [31] reported the optical characteristics of nanocrystalline cellulose (NCC) and poly (3,4-ethylenedioxythiophene) (PEDOT) thin films for use in plasmonic sensing. They determined the optical properties of composite materials and observed that the absorption spectra of NCC, PEDOT, and NCC/PEDOT thin films, measured at various wavelengths spanning from 220 to 700 nm, are differed in the absorbance value. Figure 2.5 (a) shows the spectra for PEDOT, which indicate the greatest absorbance value of 3.90 at 268 nm and 280 nm, whilst the absorption band is approximately at 260 nm to 280 nm.

The absorbance value of the NCC/PEDOT thin film at 279 nm is roughly 4.19, which is the highest among the others. They also calculated the optical band gap ( $E_g$ ) using the Tauc relation extrapolating the plot of  $(h\nu)^2$  versus  $h\nu$ , as shown in Fig. 2.5 (b), where



PEDOT has an optical band gap of 4.122 eV. Furthermore, this study was the first to describe the use of an optical sensor to detect heavy metal ions by combining two types of polymers, nanocrystalline cellulose and poly (3,4-ethylenethiophene). This research has broadened the possibilities for biopolymers and conducting polymer-based materials to be used as a sensing layer in sensor applications.

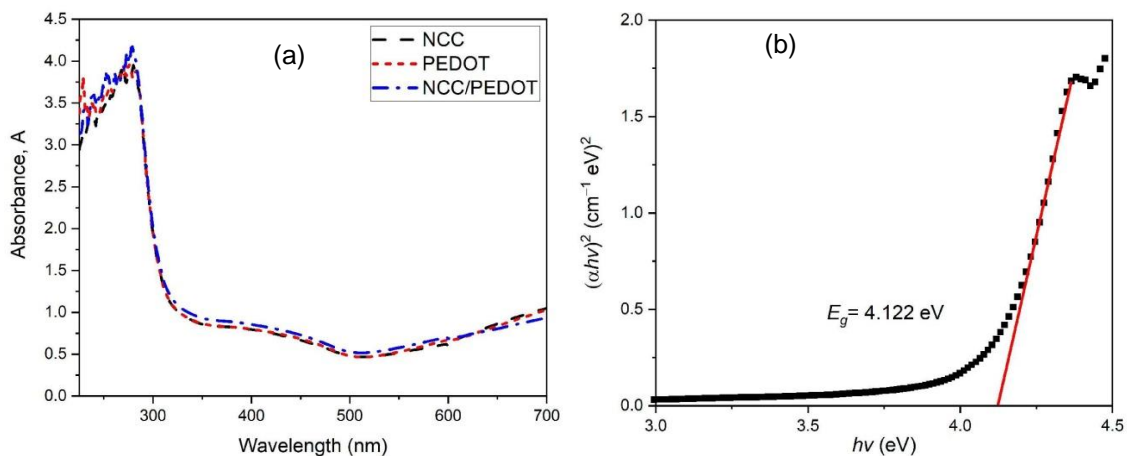


**Fig. 2.5** (a) Absorbance spectrum to wavelength of NCC, PEDOT, and NCC/PEDOT thin film, (b) bandgap energy of PEDOT thin films [31].

Nasrin *et al.* [32] studied the thickness dependent structural and surface properties of PP N-benzylaniline (PPNBA) thin films using plasma polymerization technique where the energy dispersive X-ray analysis confirms that the PPNBA films are primarily carbon and nitrogen as displayed in Fig. 2.6 (a) and (b), respectively. They have noted that wt% of several element has changed significantly after plasma polymerization, which may be due to the breakage of the bonds during the complex reaction occurred in the polymerization process.

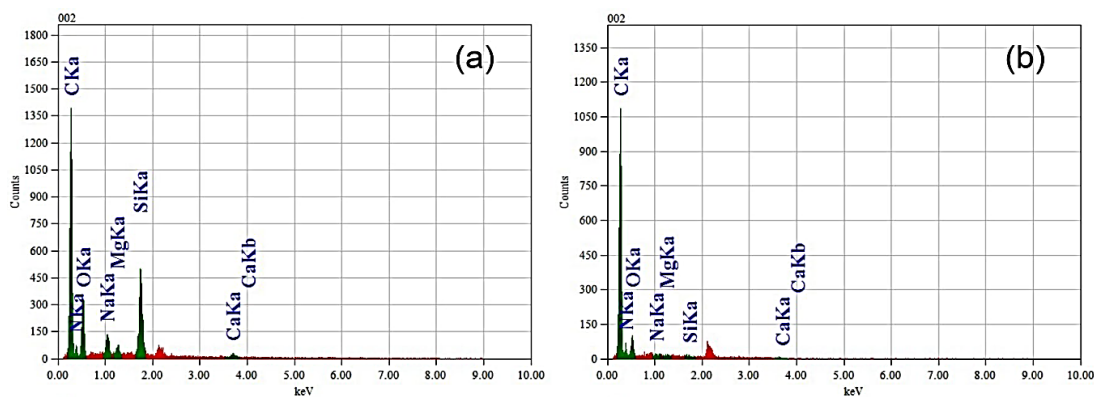


**Fig. 2.6** EDX spectra images of PPNBA thin films of thicknesses (a) 494 nm, and (b) 645 nm [32].

Sarkar and Bhuiyan [33] explored the DC conduction mechanism in the PP 1-benzyl-2-methylimidazole (PPBMI) thin films generated by glow discharge. They noticed that the chemical structure of PPBMI thin films differs from that of the monomer to some extent. The space charge limited conduction (SCLC) mechanism is prevalent in PPBMI thin films, according to  $J$ - $V$  (Fig. 2.7 (a-b)) properties of different thicknesses at various temperatures. The activation energy for conduction is determined to be 0.43 eV. Carrier mobility, free carrier density, and trap density are  $1.481018$  to  $6.351018$   $\text{m}^2 \text{V}^{-1} \text{s}^{-1}$ ,  $1.591023$  to  $5.851023$   $\text{m}^{-3}$ , and  $2.501024$  to  $5.001023$   $\text{m}^{-3}$ , respectively.

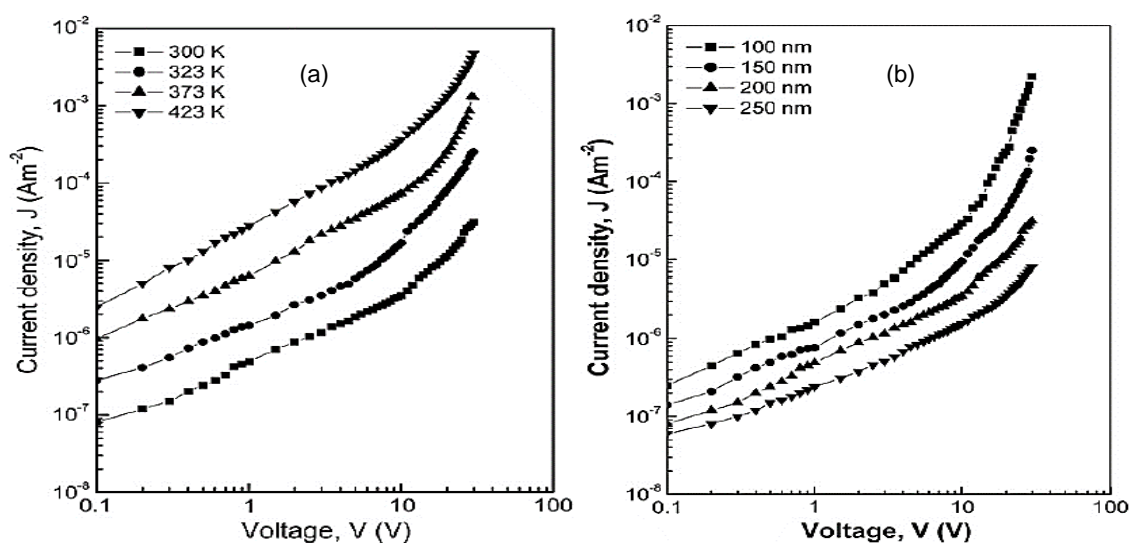


**Fig. 2.7**  $J$ - $V$  characteristics for PPBMI thin film of (a) various thicknesses at room temperature, (b) at various temperatures (thickness,  $d = 200$  nm) [33].

Manna *et al.* [34] prepared and characterized the polymerized cyclohexane thin films using RF-PECVD at different RF powers and a mixture of Argon gas and cyclohexane ( $\text{C}_6\text{H}_{12}$ ) vapor was used as the precursor. The extinction ( $k$ ) and the absorption coefficients ( $\alpha$ ) both decrease with the increase of  $\lambda$  but increases with increasing RF power as presented in Fig. 2.8 (a) and (b). Maximum values were found in the UV region and almost vanish in the infrared range, which indicates that the films are highly absorbent in the UV range and become transparent in the infrared one.

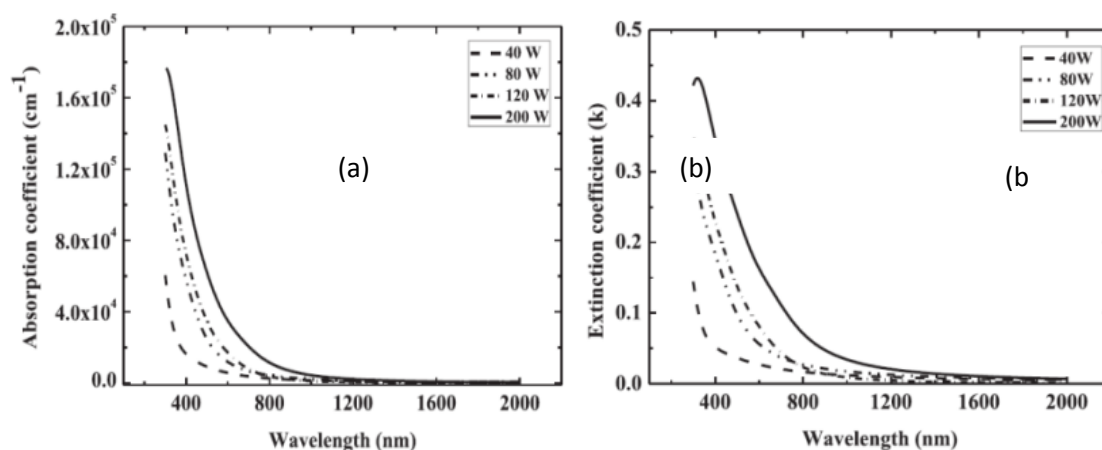


**Fig 2.8** (a) Absorption coefficient and (b) extinction coefficient  $k$  as a function of the wavelength for different RF power [34].

Momin *et al.* (2019) [35] studied optical and morphological properties of PP cyclohexane (PPCHex) thin films synthesized by using a capacitively coupled parallel plate reactor. They depict that the surface of the PPCHex thin films is smooth, homogenous, uniform and pinhole free, and thermogravimetric analyses shown in Fig. 2.9 reveal that the PPCHex films are thermally stable up to about 510 K.

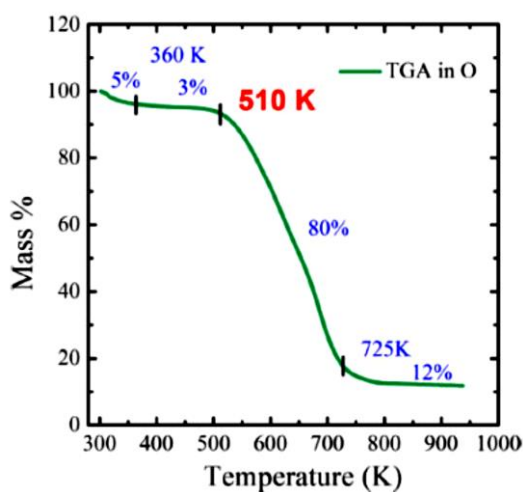


**Fig. 2.9** TGA of PPCHex in oxygen environment (scan rate 10 K/min) [35].

Giuri *et al.* [36] analyzed the rheological and physical characterization of PEDOT: PSS/graphene oxide nanocomposites for perovskite solar cells, where the thermal characteristics, determined by TGA and DSC, have evidenced a possible reduction of graphene oxide (GO), caused by the increased temperature. They verified that this is a

significant finding for solar applications since the lowering of GO might increase the composite film's stability.

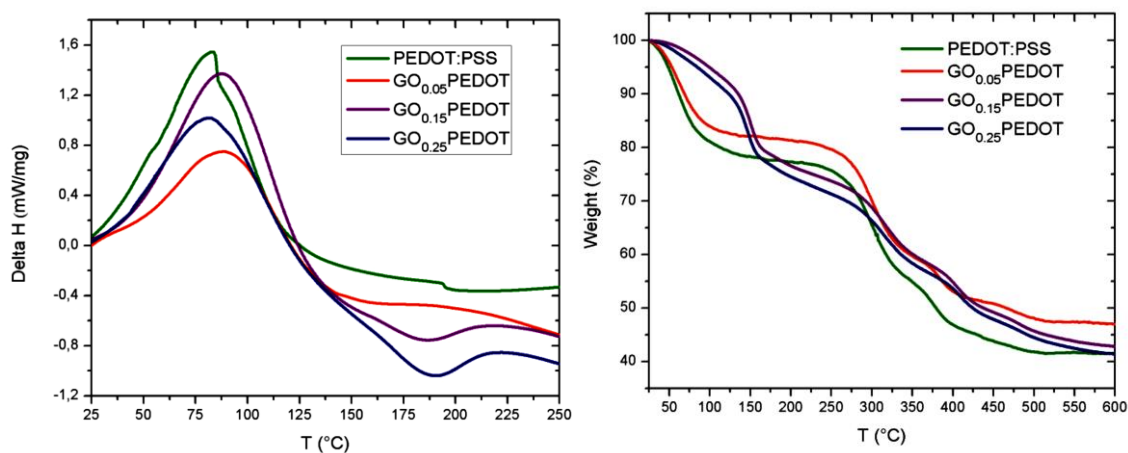


**Fig. 2.10** (a) DSC and, (b) TGA curves of the PEDOT: PSS, GO 0.05, 0.15, 0.25 PEDOT films [36].

## 2.2 Theory of Plasma Polymerization

Plasma polymers, like ordinary polymers, do not have regular repetition units and tend to create an irregular three-dimensional cross-linked network [37]. Fig. 2.11 depicts a schematic plasma polymerization arrangement. The chemical structure and physical characteristics of the traditional polymer, which is generated from the identical starting components, may be considerably different [38].

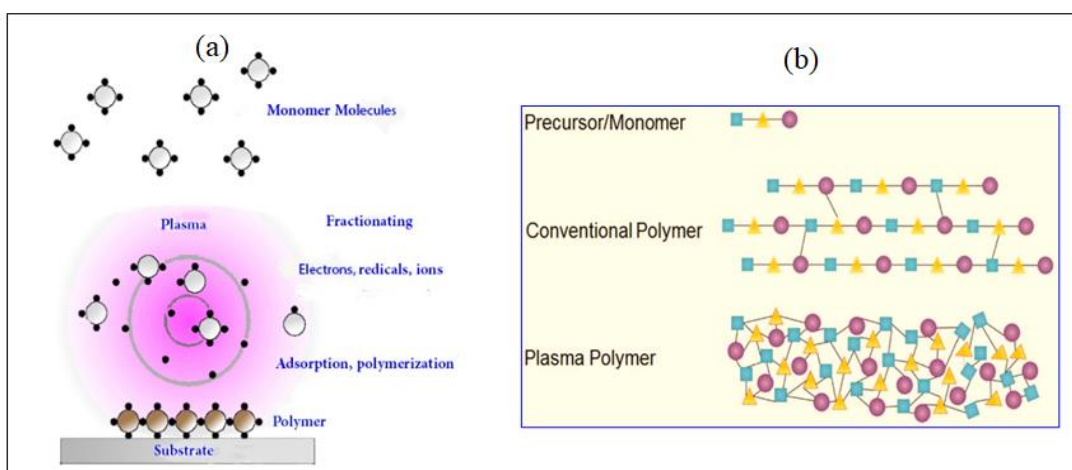


**Fig. 2.11** (a) A schematic PP configuration and (b) schematic comparison of the structures of conventional polymers and plasma polymers [37, 38].

PP is caused by a complicated process that cannot be detailed for the general situation. The deposition rate and shape of the plasma film are affected by operational factors such as monomer flow rate, pressure, frequency, and power. In all glow discharges, the

electrons or atoms created by partial ionization of molecules are the primary energy transfer sources from the electric field to the gas [39]. The PP method is generally carried out in low-temperature plasma created by glow discharges in a molecular gas at low pressure. In an evaporator, the monomer is transformed to a gas and injected into a vacuum chamber. The breaking of covalent bonds in gas phase molecules causes PP, and subsequent interactions between gas phase species and surfaces result in the deposition of polymeric materials. The gas divides into positive ions and electrons when a large potential difference between the two electrodes is introduced, resulting in a gas discharge [40, 41].

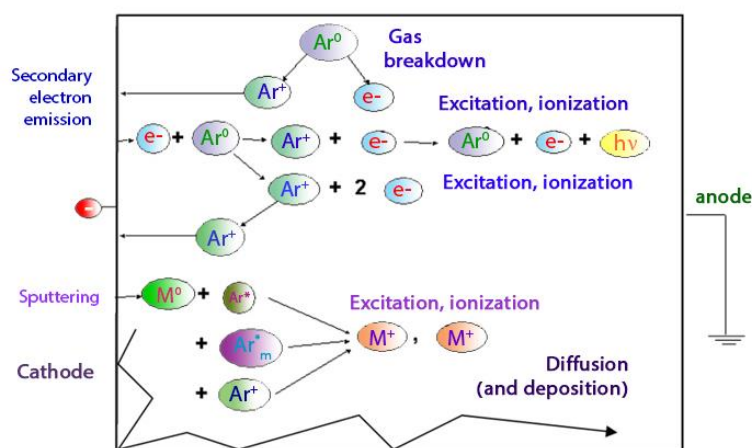


**Fig. 2.12** The schematic overview of the basic activities in a glow discharge [40].

When a potential difference is introduced, however, the electric field in front of the cathode accelerates the electrons, causing them to collide with the gas atoms. The most important collisions are inelastic collisions that induce excitation and ionization. The electric field accelerates the ions toward the cathode, where ion-induced secondary electron emission releases additional electrons. As seen in Fig. 2.12, the electrons cause fresh ionization collisions, resulting in new ions and electrons. The glow discharge plasma is self-sustaining due to the processes of electron emission at the cathode and ionization in the plasma [42].

Heating a gas or exposing it to a strong electromagnetic field can produce plasma. In general, when the energy in atoms increases, the thermal movement of atoms in solids worsens, eventually overcoming the constraining relationship between atoms in solids, such as the ionic bond, and becoming liquid. Plasmas are created in a glow discharge

system when energy is transferred from an electric field to free electrons in a low-pressure environment.

More electrons, ions, free radicals, and molecules in excited states are formed because of inelastic electron collisions with molecules, resulting in the plasma state. Plasma is an ionized gas combination made up of ions, electrons, and neutral atoms. Plasma may be created in the laboratory using a variety of methods, such as combustion flames, electrical discharges, controlled nuclear reactions, shocks, and other methods. Light discharge is the method that has piqued my curiosity the most.

### **2.2.1 Advantages of this Process**

In general PP has several benefits over conventional polymerization processes and polymerization. The most important benefit of PP is the capacity to generate polymer films of organic compounds that do not polymerize under standard chemical polymerization conditions. This approach can polymerize nearly all monomers, including saturated hydrocarbons and organic molecules that lack a polymerizable structure like a double bond. A second benefit is the simplicity with which the polymers may be applied as coatings compared to traditional coating methods. PP achieves all of these in virtually a single process, whereas covering a substrate with traditional polymers needs many phases. In comparison to traditional coatings, the resulting polymer coatings provide a variety of benefits. These benefits include being practically pinhole free, very dense, and the ability to readily vary the thickness of the coating.

### **2.2.2 Applications of PP Thin Films**

The PP thin films have become important in a variety of fields, including optics, microelectronics, and biomaterials. A few potential applications for PP thin films are listed below:

- ❖ In optical systems: Optical wave guide, anti-dimming coating, optical fiber, optical window, improvement of transparency, laser, and contact lens, etc.
- ❖ In electrical devices: Insulator, thin film dielectric and separation membranes for batteries, etc.
- ❖ In electronic devices: Integrated circuit elements, VLSI resists and in non-crystalline semiconductor and non-crystalline fine ceramic etching, PV technology, etc.

- ❖ In chemical processing systems: Anti-creasing, protective coating, scratching and adhesion improvement abrasion resistant coating, etc.
- ❖ Biomedical applications: Artificial kidney, enzyme immobilization, sterilization, and pasteurization, sustained release of drugs and pesticides, blood vessel, etc.
- ❖ In textile industries: Water repellence, anti-flammability, anti-electrostatic treatment, dying affinity, hydrophilic improvement, shrink-proofing, etc.

## CHAPTER 3

### MATERIALS AND METHOD

This chapter presents the PP process, including monomers, substrates, and a capacitively connected glow discharge PP setup for polymer synthesis. FESEM, EDX, FTIR, UV-Vis spectroscopy, TG/DSC and DC electrical measurements are among the methods used to characterize PPEDOT thin films.

#### 3.1 Monomer

The organic monomer 3,4-ethylenedioxythiophene, commercial named EDOT ( $C_6H_6O_2S$ , Sigma-Aldrich, 97%), has been purchased from Germany. Basically, EDOT has been chosen because of its high conductivity, medium boiling points and toxic-free, etc. and several properties of EDOT are presented in Table 3.1. This monomer is widely used as a precursor to form PEDOT, which is applied in electrochromic displays, photovoltaics, electroluminescent displays, printed wiring, and sensors [44]. The chemical structures of EDOT and predicted PEDOT are displayed in Fig. 3.1.

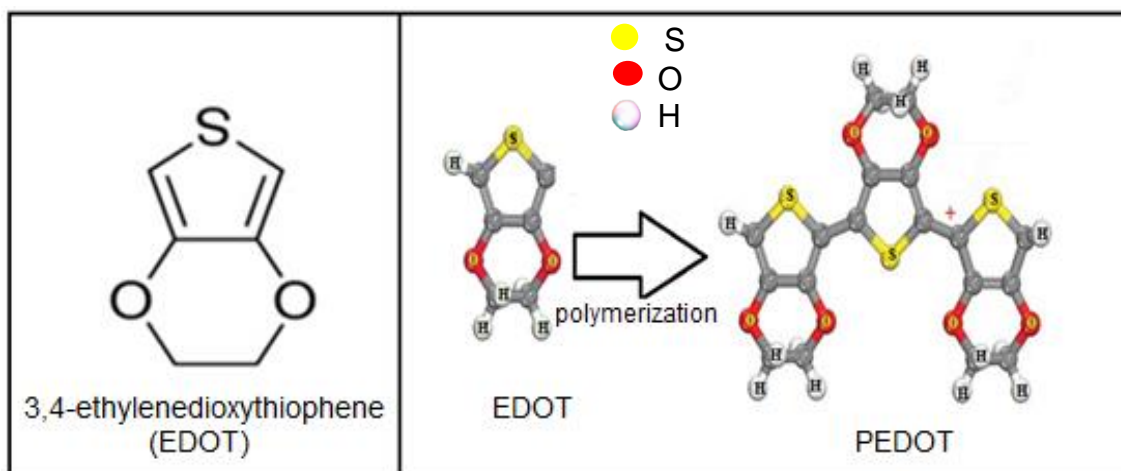


**Fig. 3.1** The chemical structure of EDOT and PEDOT [44].

#### 3.2 Substrate and Its Cleaning

The glass substrates (Sail Brand, China), in which films were deposited and a monomer container 10 ml (Pyrex) and other necessary equipment were collected from the local market. Firstly, the glass substrates were resized by a cutter and cleaned with detergent. To get a homogeneous, smooth, and flawless thin polymer film, it is essential that after keeping in detergent for about 15 minutes, slides were cleaned with distilled water and



these cleaned slides were rinsed with acetone and finally cleaned by ultrasonic bath. These cleaned glass slides were rinsed with deionized water and dried by a drier before deposition.

**Table 3.1** General properties of 3,4-ethylenedioxythiophene.

IUPAC name	3,4-ethylenedioxythiophene
Molecular formula	C <sub>6</sub> H <sub>6</sub> O <sub>2</sub> S
Physical state	Liquid
Color	Colorless monomer
Toxicity	Non-toxic
Molecular weight	142.18 g/mol
Boiling point	193 °C at 760 mm Hg
Density	1.34 g/cm <sup>3</sup>
Refractive index	1.5765

### 3.3 PP Set-up and Deposition Process

The glow discharge PP set-up consists of plasma reaction chamber, electrode system, pumping unit, vacuum pressure gauge, and input power for plasma generation, monomer injection system and a flow meter. Generally, the plasma glow is produced around two electrodes attached with a capacitively coupled system, where the ultrasonically cleaned and dried glass substrates were placed on the lower electrode. These electrodes consist of stainless steel, which are smooth and placed with parallel position. The distance between two plates is kept 0.038 m. The diameter and thickness of the plates are 0.09 m and 0.001 m, respectively.

A rotary pump was applied to pump down the reactor chamber up to 9.33 Pa very slowly. The plasma glow was generated powering these two parallel plates using AC (50 Hz) or RF (13.56 MHz) power. The monomer tube including the monomer container was heated up to 75 °C using hairdryer to prevent condensation of EDOT vapor. As a result, monomers can easily be injected into the plasma reactor. The monomer flow rate was adjusted by a fine injection valve. Chamber pressure remains stable at about 17.3 Pa during deposition when AC power is applied but it increases up to 26.67 Pa when RF power is applied. Remaining constant input power of about 37-watt AC and 37-watt RF, the monomer molecules were started to absorb and condensed

onto the substrates and finally after 30 to 60 minutes of deposition, the PPEDOT thin films were formed onto the glass substrates.

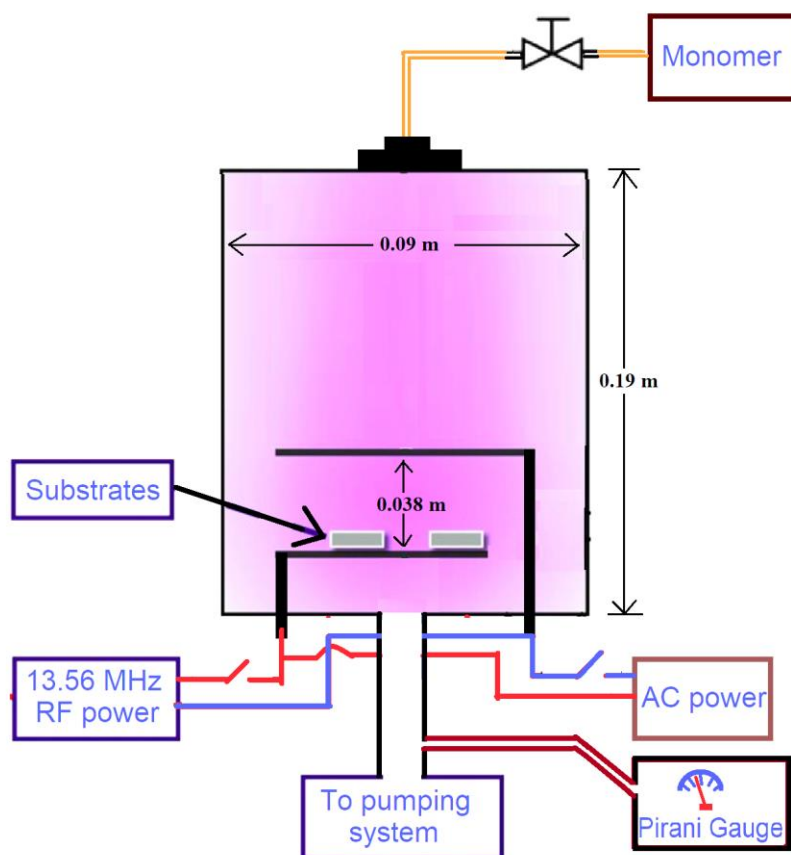


**Fig. 3.2** Schematic diagram of the PP set up in laboratory.

The color of plasma changed when monomer vapor was injected into the chamber, as illustrated in Fig. 3.3 (a) and (b), respectively. At a constant AC and RF discharge power of 37 W, the deposition period was adjusted from 30 to 60 minutes to obtain PPEDOT thin films of various thicknesses. Finally, prepared PPEDOT samples are ready for characterization as shown in Fig. 3.3 (c).

Generally, using AC plasma power, polymer thin films have been prepared in plasma polymer and nanocomposite (PPNC) lab, department of Physics, BUET. No comparative study is found using AC and RF plasma to deposit organic thin films. Again, a well-developed RF plasma generator (13.56 MHz) is available in PPNC lab. Besides, preparing thickness dependent PPEDOT thin films, it is focused to develop RF PPEDOT thin films so that it can be compared what's different properties will be detected between AC and RF films. Finally, it is concluded which films are best and the RF generator will be used as alternative power source to AC plasma. As a result, AC and RF plasma power is used in this study.

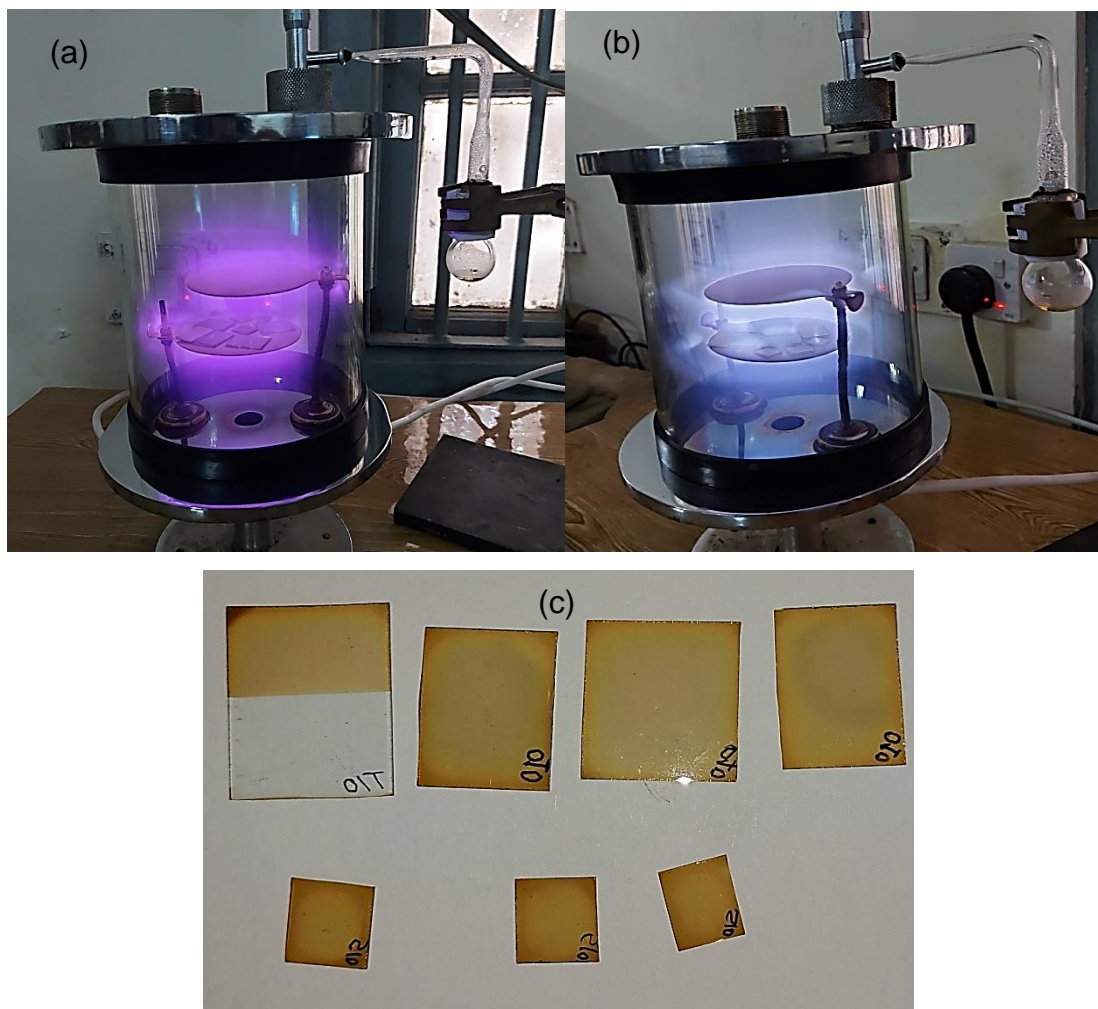


**Fig. 3.3** Glow discharge plasma: (a) before deposition (b) during deposition, and (c) prepared PPEDOT samples.

The following optimization conditions are used in this study:

**Table 3.2** Optimized conditions for thin film deposition.

Experimental condition	Name/Values	
	AC plasma	RF plasma
Electrode distance	3.8 cm	3.8 cm
Position of the substrate	Lower electrode	Lower electrode
Deposition power	37 W	37 W
Pressure before deposition	9.33 Pa	9.33 Pa
Pressure during deposition	17.33 Pa	26.67 Pa
Deposition time	30 - 60 min	30 min
Frequency	50 Hz	13.56 MHz

### 3.4 Thickness Measurement

A sample may be thick or thin film. Basically, it can be confirmed by measuring its thickness. The characteristics of a film such as optical properties, electrical properties are widely dependent on films thickness, therefore thickness measurement of a thin film is very important. In this study, thicknesses of the deposited films are measured by a multiple beam interferometer device with the help of theories of Tolanskey [53]. A schematic diagram of the multiple-beam interferometer based on Fizeau fringes is shown below in Fig. 3.4. This device is developed on the principle of Fizeau fringe which is based on separated amplitude interference and thickness of the film's " $d$ " was determined by the equation 3.1 [54].

$$d = \frac{\lambda b}{2 a} \dots\dots\dots (3.1)$$

where,  $\lambda$  is the wavelength of sodium light and the value of  $\lambda$  is 589.3 nm, and  $\frac{b}{a}$  is the fractional discontinuity identified in Fig. 3.4.

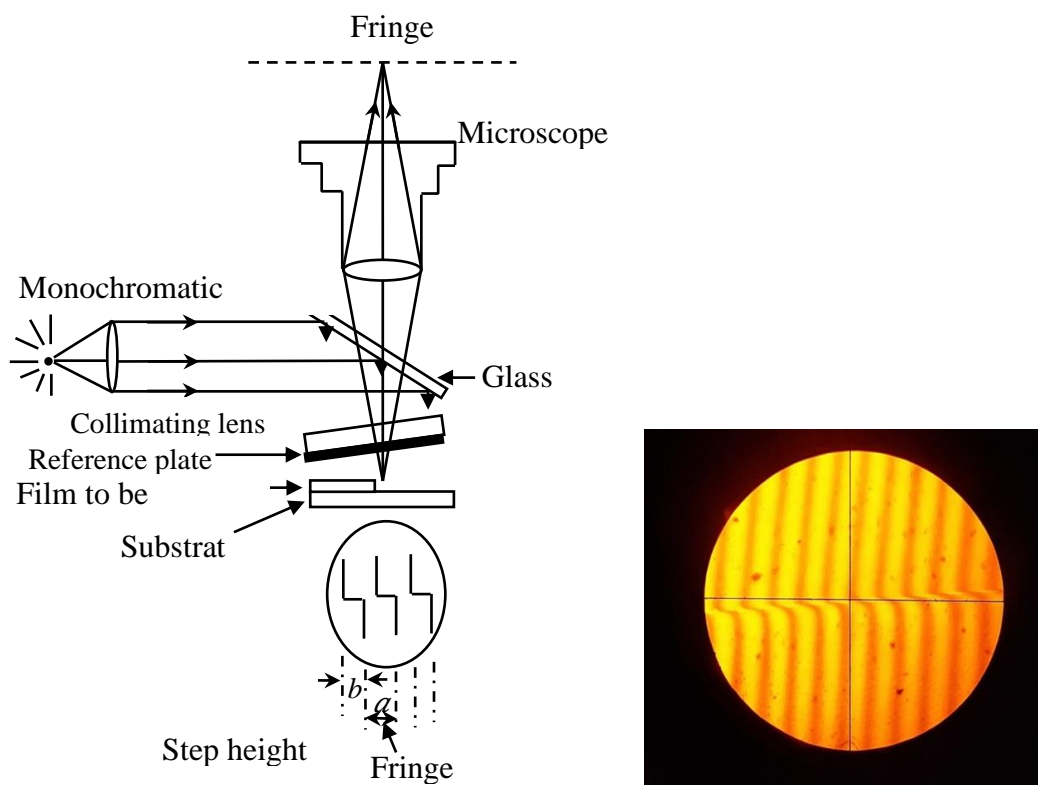


**Fig. 3.4** Diagram of Fizeau interferometer used for the measurement of thin film thickness (Inset: Fizeau fringe pattern of the PPEDOT thin films).

Thicknesses were determined for the samples prepared at different deposition times and different power sources from different position and averaged from at least 5 thicknesses.

It is observed that film thickness is increasing with increasing deposition time. With varying power sources like AC and RF, thickness also changed, but randomly. The thicknesses of AC samples were determined to be vary between 250 nm and 390 nm but for RF samples the thickness is 690 nm at a constant power about 37 watt. The film thickness of RF samples is increased notably as comparative to the AC samples despite all remaining parameters being constant. It may happen due to the fragmentation or etching of monomer during polymerization. However, in this observation, it can be said that the deposition rate of RF samples becomes higher than AC samples.

### 3.5 Electroding Process

For electrode deposition, aluminum (Al) (purity of 4N British chemical standard) was utilized. Al has been shown to have excellent adherence to glass slides [45]. Al film has the advantage of being able to self-heal defects in sandwich structure [46]. A Hind High vacuum coating unit (Model -12A4D, India) was used to deposit the electrodes. An oil diffusion pump supported by an oil rotary pump emptied the system to a pressure of less than  $10^{-5}$  Pa. A metal rod of length 0.1 m was set above the tungsten filament, which supported the glass substrates with mask, and Al was retained on the tungsten filament. A low-tension power source, capable of producing 100 A current at a potential drop of 10 V, was used to heat the filament.

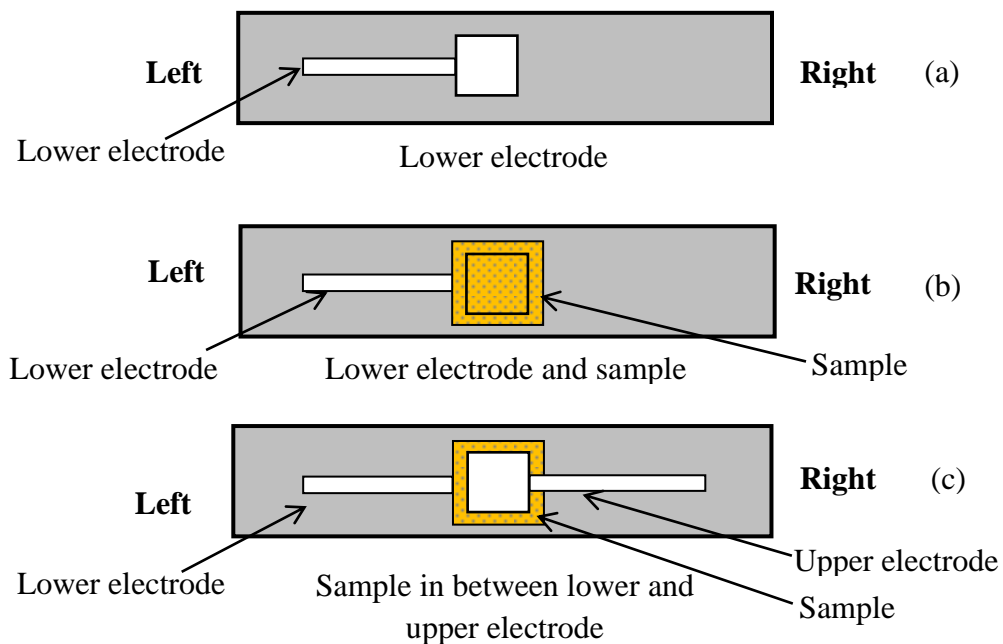


**Fig 3.5** Electrode assembly: (a) Lower electrode, (b) lower electrode and the sample, (c) sample in between the upper and lower electrode [45].

The water flowed continually to keep the diffusion unit cold. After evacuating roughly  $10^{-5}$  Pa, the Al was heated with a low-tension power source until it melted. The Al was vaporized, and thus the bottom electrode was placed on the glass slide. Al coated glass substrates were removed from and put in the middle of the lower electrode of the plasma deposition chamber for optimal EDOT thin film deposition. As shown in Fig. 3.5, the upper Al electrode was likewise produced on the PPEDOT film.

### **3.6 Characterization Techniques**

In this work, the plasma polymerized thin films have been characterized by different experimental techniques. The techniques are given below:

#### **3.6.1 FESEM and EDX**

The surface morphology of the produced thin films was observed using an FESEM (Model JEOL JSM 7600F, USA). With the use of a gold sputtering coater, the PPEDOT thin films were coated with a thin coating of gold to avoid the charging effect during FESEM. EDX studies linked to the FESEM have also corroborated the compositional components of the films.

#### **3.6.2 FTIR spectroscopy**

FTIR spectra of the samples were recorded by using a double-beam FTIR spectrometer (Model: SIMADZU, FTIR-8400) to identify different types of vibration of bonding in the films and to elucidate chemical structure of the EDOT and PPEDOT, FTIR spectra of the liquid monomer and the polymer thin films in powder form (which is collected from the substrate by scrapping method) were taken in the wavenumber range of  $400 - 3500 \text{ cm}^{-1}$ .

#### **3.6.3 UV-Vis spectroscopy**

A double beam UV-Vis spectrophotometer (Shimadzu UV-2600, Japan) was used to measure the optical absorbance, transmittance, and reflectance of PPEDOT thin films deposited on glass substrates in the wavelength range of 300 - 800 nm, which was used to calculate the optical bandgap energy and other important optical parameters such as absorption coefficient, extinction coefficient, Urbach energy, steepness parameter, refractive index, and so on. A comparable blank glass slide was utilized as a reference throughout the measurement.

### 3.6.4 Differential thermal and thermogravimetric analysis

Thermogravimetric analysis (TGA) was used to study the thermal stability of the PPEDOT thin films using a computer-controlled TG/DSC (Model: NETZSCH STA 449 F3 Jupiter®) thermal analysis equipment. A horizontal system balance mechanism is used in the TGA/DSC model. In nitrogen, the heating rate was 10 K/min. Throughout the tracing procedure, alumina was employed as a reference material.

### 3.6.5 DC electrical measurement

Sandwiched type Al/PPEDOT/Al samples were created using a metal coating equipment (Edward 306, England) at a pressure of around  $1.33 \times 10^{-3}$  Pa and an effective Al electrode area of  $10^{-4}$  m<sup>2</sup> for DC electrical tests. To measure the current across the thin films, a high impedance electrometer (Model: 614, Keithley Instruments Inc., USA) was used, and DC voltage was supplied by a stabilized DC power supply (Model: 6545A, Agilent, Japan). The DC measurements were carried out at various temperatures (298, 308, 318, 328, 338, 348, 358 and 373 K) that were kept constant. A Chromel-Alumel thermocouple coupled to a digital micro voltmeter was used to record the temperature of the samples (Model: 197A, Keithley Instruments, USA).

When an electrical field is applied to a polymer, any charges in the polymer will redistribute if they are mobile enough to respond in the time scale of the applied field. The variation of current density with voltage in a material can be expressed by a power law generally,  $J \propto V^n$  where,  $n$  is a power factor [47]. Generally, two conduction mechanism is found in polymer thin film, like Ohmic and non-Ohmic, when  $n$  is unity, the conduction is Ohmic and the value of  $n$  is less or more than unity, then the conduction process is not Ohmic. Thermal or Schottky effect, space-charge-limited conduction (SCLC), and Poole-Frenkel (PF) conduction are the three most likely mechanism processes identified in polymer thin films [48, 49]. This three-type conduction mechanism are briefly described in below:

Schottky emission is a conduction process in which electrons in the metal transcend the energy barrier at the metal dielectric interface to go to the dielectric if they gain enough energy via thermal activation. The image force has the potential to reduce the energy barrier height at the metal dielectric contact. The image force-induced barrier-lowering effect is known as the Richardson-Schottky (RS) or Schottky effect [48]. In the

Schottky mechanism, the current density,  $J$  is proportional to the square root of the applied field.

When an electric field is given to a sample, the potential barrier height induced by an atom's Coulombic forces is lowered. The Poole-Frenkel (PF) effect describes this occurrence [48].

The lower potential energy may enhance the likelihood of an electron being thermally pushed out of the trap and into the conduction band of the dielectric. The space charge injected into the insulator's conduction band can carry current, and when the transport is slower than the generation, it becomes the rate-determining step, and the conduction is described by the SCLC theory [49].

Differentiation between the types of the electronic conduction mechanism can be done by investigating the dependence of  $J$  on film thickness. The relation  $d (J \propto d^{-l})$  for the samples of different thickness at a constant voltage, where  $l$  is the parameter dependent on the trap distribution within the material. The value of the slope,  $l < 3$  indicates PF or RS conduction is present in the material, while  $l \geq 3$  indicates the possibility of SCLC [50].

The temperature dependency of the current density,  $J$ , is investigated using the Arrhenius equation. The activation energies are evaluated in the two temperature regions at the higher ( $V = 60$  V) and lower ( $V = 10$  V) voltages from the slopes of  $J$  versus  $1/T$  curves [51].



## CHAPTER 4

### RESULTS AND DISCUSSION

This chapter has presented the findings of several experimental investigations done on as-deposited thickness dependent PPEDOT thin films. FESEM, EDX, FTIR, UV-Vis spectroscopy, and TG/DSC were used to examine the surface morphological, elemental, structural, optical, and thermal characteristics of PPEDOT thin films. DC electrical measurements are also used to investigate the DC electrical conduction mechanism in the PPEDOT thin films. Finally, a comparison study between AC and RF PPEDOT films have been discussed.

#### 4.1 Surface Morphology and Compositional Analyses

##### 4.1.1 FESEM study

The characteristics of the conducting polymer layer can be influenced by the surface morphology of the coated dielectric layer [52]. The surface morphology was studied by FESEM of the PPEDOT thin films prepared onto glass substrates taken various points at an accelerating voltage of 5 kV at different magnifications presented in Fig. 4.1 and 4.2, respectively. From lower to higher magnifications, of the PPEDOT thin films of thickness 330 nm surfaces are observed to be smooth, pinhole-free, scratch-less, flawless, homogeneous as shown in Fig. 4.1 (a)  $\times 20$  k, (b)  $\times 30$  k, (c)  $\times 50$  k and (d)  $\times 100$  k. During the growth of the thin films, monomer molecules are placed on substrate uniformly owing to interaction among the molecular chains. Throughout the FESEM images, a few small white spots were visualized at lower magnification which may be dust coming from environment. Kabir *et al.* also showed similar surface micrographs for plasma polymerized pyromucic aldehyde films deposited by using a capacitively coupled glow discharge system [53].

With increasing film thickness, the surfaces of PPEDOT thin films also remain smooth, pinhole-free and homogeneous as shown in Fig. 4.2. No significant change is observed in different thicknesses of 250 nm, 330 nm, and 390 nm at a constant magnification.

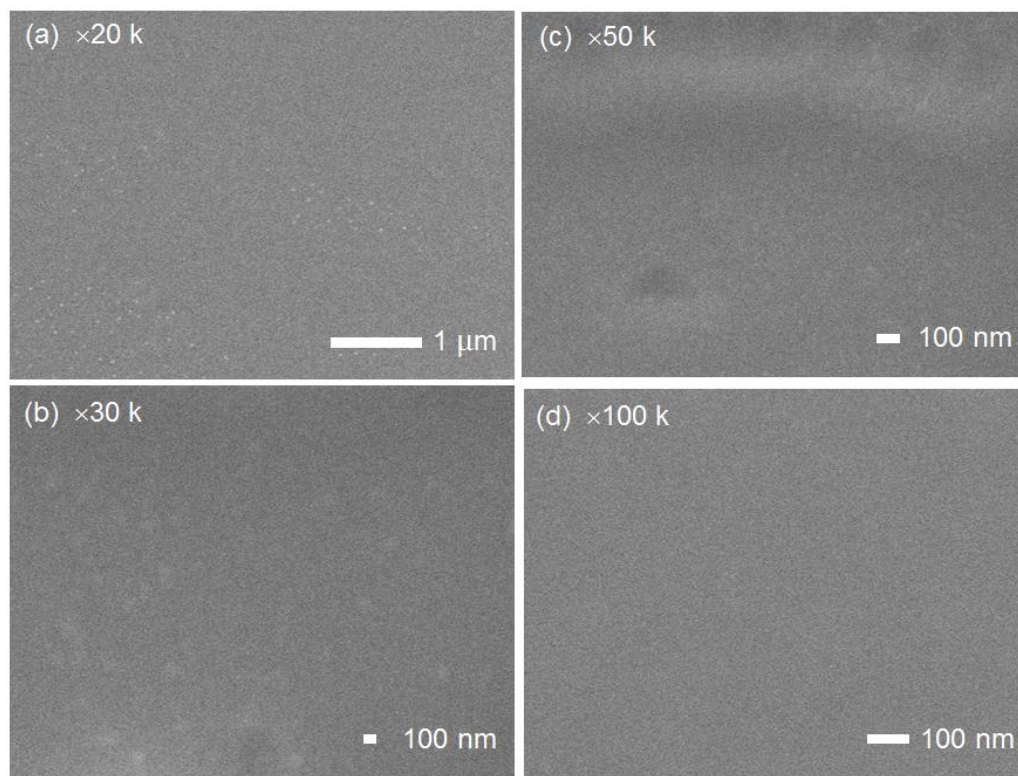


**Fig. 4.1** FESEM micrographs of the PPEDOT (AC) thin films at different magnifications of thickness 330 nm, (a) × 20 k, (b) × 30 k, (c) × 50 k, (d) ×100 k.

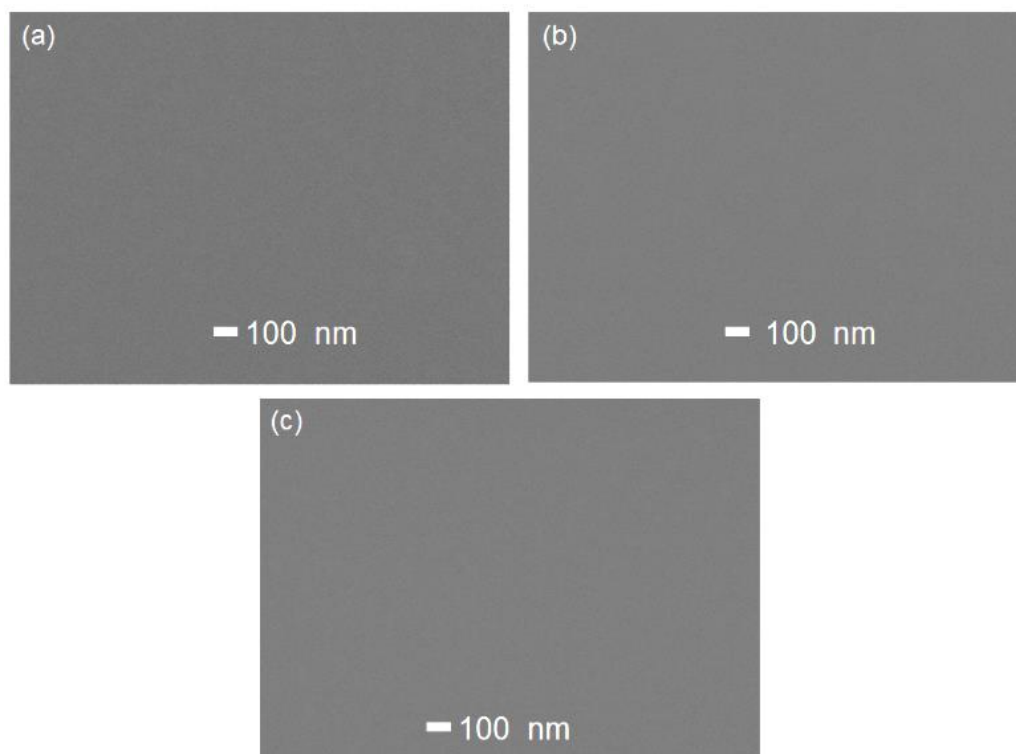


**Fig. 4.2** (a), (b), (c) FESEM micrographs of the PPEDOT thin films at thicknesses of 240 nm, 330 nm and 390 nm at magnification of × 50 k, respectively.

#### 4.1.2 EDX analyses

To indicate mass percentages of the constituent elements of PPEDOT thin films, EDX spectra analysis were performed which was attached to the FESEM. The EDX spectra of the as-deposited PPEDOT thin films are shown in Fig. 4.3 for the films fabricated by AC plasma polymerization technique, respectively.

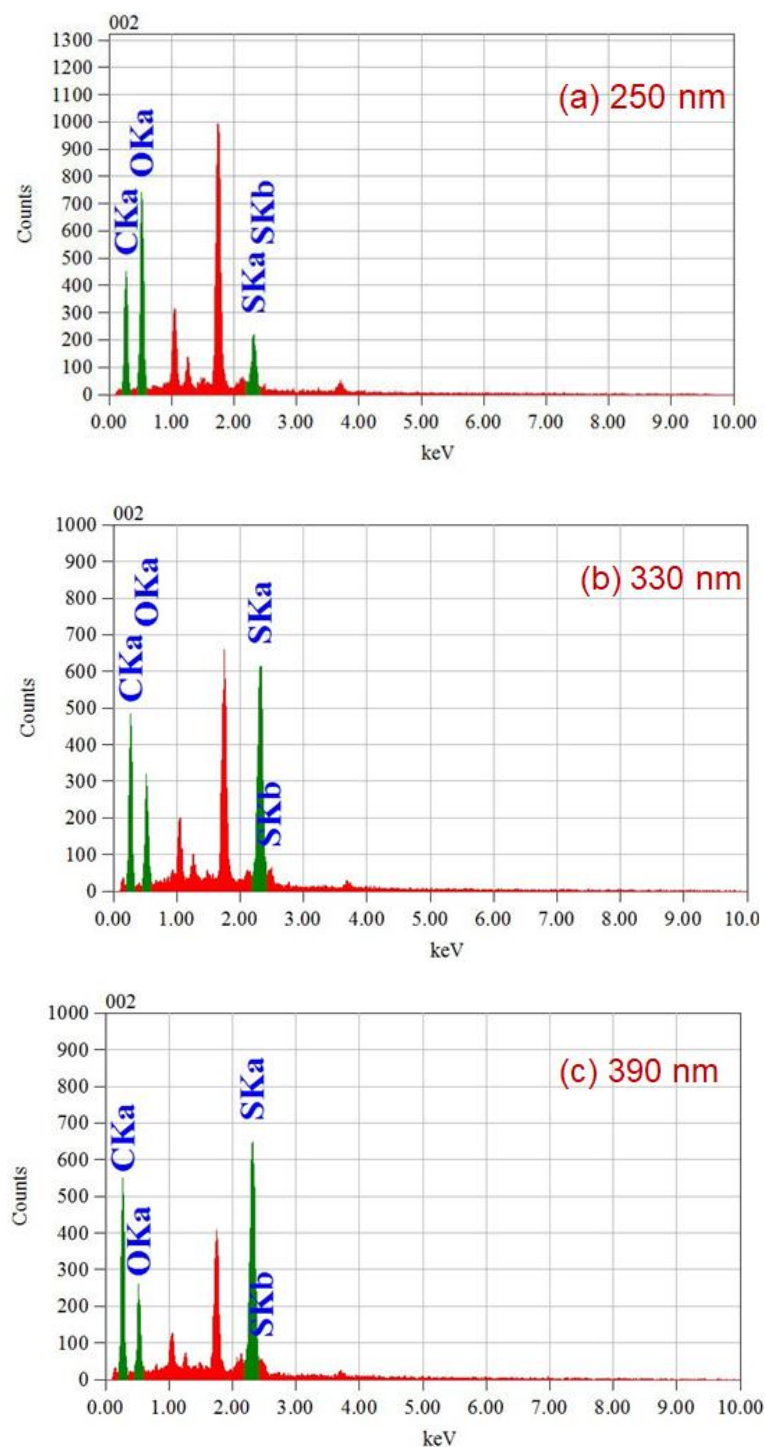


**Fig. 4.3** EDX spectra of the PPEDOT thin films of thicknesses (a) 250 nm, (b) 330 nm, (c) 390 nm, respectively.

The atomic percentage (at%) of constituent elements of PPEDOT thin films are listed in Table 4.1. The at% of C in the PPEDOT thin films increases as the film thickness increases, which might be due to hydrogen loss during the plasma polymerization process.

**Table 4.1** Atomic percentage (at%) of the elements present in the PPEDOT thin films.

Element detected	Elements in PPEDOT (at%)		
	250 nm	330 nm	390 nm
C	51.51	71.05	75.11
O	44.36	18.82	14.89
S	4.13	10.13	10.00
H	Not detected	Not detected	Not detected
Total	100.00	100.00	100.00

This observation shows the presence of carbon (C), oxygen (O) and sulfur (S) in PPEDOT thin films. Although EDOT monomer consists of C, H, S and O, but H is not detected because EDX cannot detect the presence of H, a limitation of this method. It is noticed here that the polymer contains no extra elements as mentioned in EDX data Table 4.1, which confirmed the purity of the PPEDOT thin films as detected same elemental atomic percentage in literature review part [28].

#### 4.2 Structural Analyses: FTIR Spectroscopy

To identify and investigate the presence of various functional groups in polymers FTIR analysis is one of the powerful techniques [54]. The FTIR spectra of EDOT, PPEDOT (AC) at room temperature are presented in transmittance mode ranging from 3500 to 500  $\text{cm}^{-1}$  wavenumber that is shown in Fig. 4.4. These spectra confirm that the chemical structures of the deposited films are changed due to AC plasma polymerization and the structure of PPEDOT departs from that of the monomer structure.

The intensity of the absorption bands detected from FTIR spectrum of the PPEDOT has decreased significantly compared to that of the monomer spectrum. It may be due to an implication of reorganization of the  $\pi$ - $\pi$  interactions to monomer molecules during plasma polymerization. In the variation of thickness, FTIR spectra shows almost similar absorption peaks. Table 4.2 presents the principal vibrational absorption peaks in the spectra and their tentative assignments.

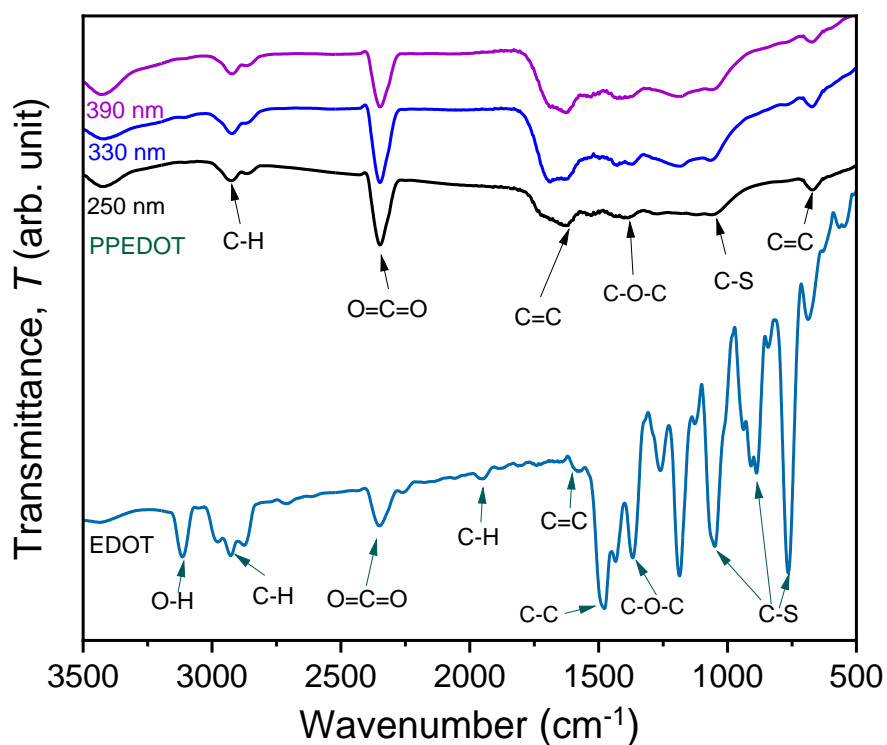


**Fig. 4.4** FTIR spectra of EDOT monomer; as-deposited PPEDOT (AC) thin films at various thicknesses.

**Table 4.2** The FTIR spectroscopic assignments of the EDOT monomer and PPEDOT (AC) thin films.

Assignment	Wavenumber (cm <sup>-1</sup> )			
	Monomer EDOT	PPEDOT (AC) thin films		
		250 nm	330 nm	390 nm
O-H stretching	3113	----	----	----
C-H stretching	2934	2926	2930	2932
O=C=O stretching	2357	2343	2347	2351
C-H bending	1951	----	----	----
C=C stretching	1584	1620	1623	1620
C-C stretching	1471	----	----	----
C-O-C	1365	1377	1387	1387
C-S ring stretching	1053, 890, 760	1045	1048	1053
C-H	661	662	670	670

In the spectrum of the monomer O-H, C-H bands appeared at 3113, 2934 cm<sup>-1</sup> indicate the presence of -CH<sub>2</sub> asymmetric stretching and -CH<sub>2</sub> symmetric stretching vibrations,

respectively [55]. These peaks confirm hydrocarbon ions in the structure. The stretching band of C-H in PPEDOT corresponding to  $2934\text{ cm}^{-1}$  shifted very slightly towards higher wavenumber.

The PPEDOT (AC) contains a broad spectrum assigned around  $2347\text{ cm}^{-1}$ , which corresponds to O=C=O stretching mode. The absorption peaks observed at  $1951\text{ cm}^{-1}$  in the EDOT spectra appear due to the C-H bending vibrations. The peaks that arise around  $1584\text{ cm}^{-1}$  in EDOT and  $1620\text{ cm}^{-1}$  in the PPEDOT spectra show the presence of conjugation i.e., C=C stretching vibrations. The absorption peak in the monomer such as the band at around  $1471\text{ cm}^{-1}$  for asymmetric C-C indicates the inter-ring stretching in thiophene characteristics, and absorption peaks around  $1365\text{ cm}^{-1}$  in monomer and approximately  $1377\text{ cm}^{-1}$  in PPEDOT indicates the presence of C-O-C stretching vibrations modes in ethylendioxy groups. Additionally, the C-S of thiophene backbone is also presented at the sharp absorption peak at about  $1053\text{-}890\text{ cm}^{-1}$ , which is attributed to C-S ring vibration disappear in the PPEDOT spectra [31].

These clearly suggest that the chemical structure is modified or changed during the plasma polymerization. The absorption band at  $661\text{ cm}^{-1}$  corresponding with C-H out of plane bending is shifted to higher wavenumber of  $\sim 662\text{ - }670\text{ cm}^{-1}$  in the spectrum of PPEDOT (AC), clearly indicating the conjugation in the chemical structure [56].

### 4.3 UV-Visible Spectroscopic Analyses

UV-Vis spectroscopic analysis is the most powerful approaches to study the energy band graph of crystalline materials as well as amorphous materials [57]. The optical absorption spectra of PPEDOT thin films as synthesized with AC power was investigated to analyze several optical parameters including absorbance, transmittance, absorption co-efficient, optical band gap, Urbach energy, steepness parameter, extinction co-efficient, refractive index, optical conductivity, and skin depth, which are carried out in the wavelength range of 200 nm to 800 nm at room temperature.

Fig. 4.5 shows the variation of absorbance as a function of wavelength of the PPEDOT thin films. The absorbance is increased with increasing film thicknesses. In the UV-Vis region, the absorbance upturns sharply and reaches a maximum value at about wavelength 270 nm then falls rapidly up to about 375 nm for all the PPEDOT thin

films. Finally, the value of all absorbance spectra changes very slowly and becomes almost constant at about 550 nm wavelength as displayed in Fig. 4.5.

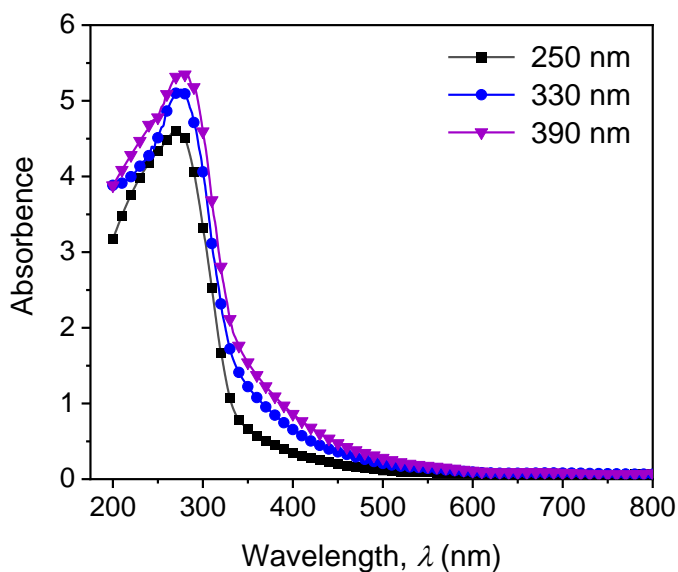


**Fig. 4.5** Spectral distribution of absorbance of PPEDOT (AC) films.

Peak values of absorbance for all samples are placed in lower wavelength region due to the presence of the  $\pi$ - $\pi$  conjugation. In addition, the maximum value of absorbance rises with the increase of film thickness due to increase of the carbon contents or it may be happened an increase in scattering with increasing thickness.

The optical transmittance graph of the PPEDOT thin films is presented in Fig. 4.6 as a function of wavelength.

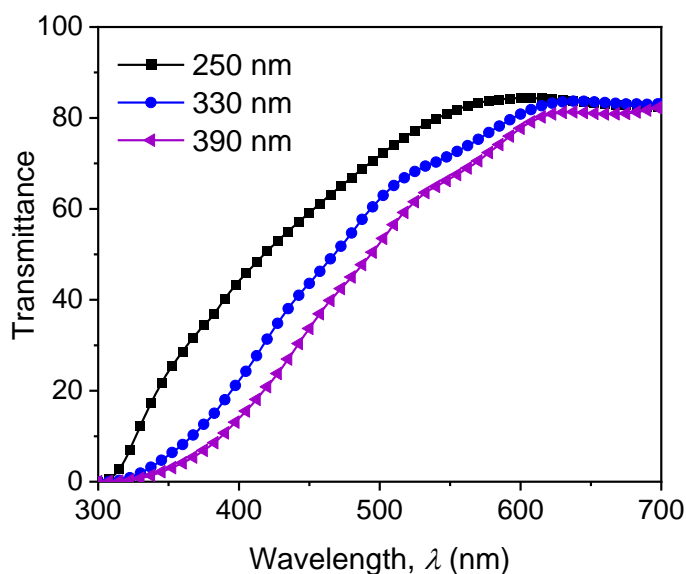


**Fig. 4.6** Spectral distribution of transmittance of PPEDOT (AC) films.

Transmittance increases with increasing wavelength at lower range (350 –550 nm) and finally reaches almost a constant value at higher wavelengths (600 –800 nm). In lower wavelength region, the sample shows slightly low transmittance, but it shifts quickly to 86% transmittance at ~ 575 –735 nm wavelengths. That’s why, it can be confirmed that all the films are transparent in the visible region. It is also found that transmittance increases with increasing thickness due to high crosslinked density [58].

The absorption coefficient ( $\alpha$ ) was determined by Eq. 4.1 [57] where  $\alpha$  is calculated by absorbance,  $A$ , and the path length of the absorbed specified, as denoted by film thickness  $d$ .

$$\alpha = \frac{2.303 A}{d} \quad (4.1)$$

Here,  $A = \log_{10} \left( \frac{I_0}{I} \right)$  with  $I_0$  is the incident beam intensity and  $I$  is the transmitted beam intensity. Fig. 4.7 represents the absorption coefficient graph to photon energy. The greater the absorption rate, the less amount of light will reach into a substrate prior to absorption. The absorption changes with photon energy following an exponential fall in the low energy region, which is caused by the lack of long-range order films or existence of defects [58].

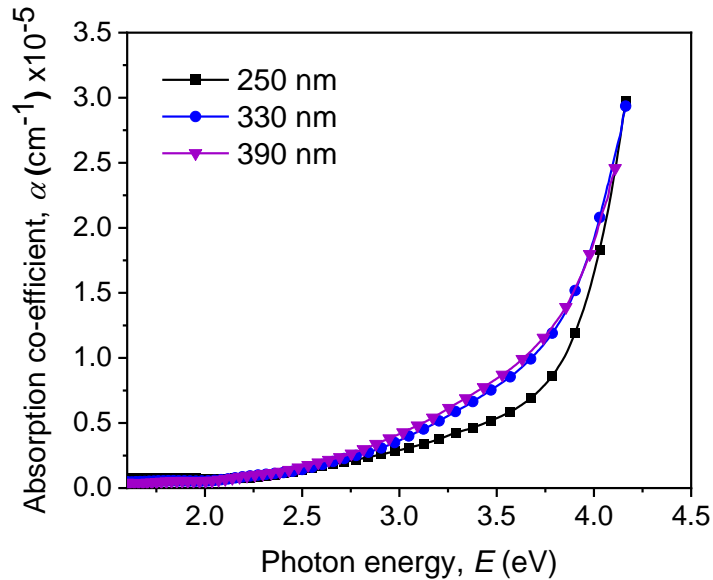


**Fig. 4.7** Plot of absorption coefficient,  $\alpha$  with  $h\nu$ , for as-deposited PPEDOT thin films of different thicknesses.

The optical band gap,  $E_g$ , is expressed the optical transitions of a material possession, which is one of the most important optical parameters related to the electronic structure



of a film. The well-known Tauc relation is used to evaluate the allowed optical band gaps,  $E_g$  of the PPEDOT thin films, [58], which is mentioned below.

$$\alpha h\nu = C (h\nu - E_g)^n \quad (4.2)$$

Where, the Tauc parameter  $C$  indicates the proportionality factor,  $h\nu$  indicates the photon energy and the index  $n$  indicates the nature of optical transition.

The direct bandgap,  $E_{g(d)}$ , is calculated using the following equation where  $n = 1/2$  corresponding the intercept of the linear part of the curves  $(\alpha h\nu)^2$  versus  $h\nu$  as shown in Fig. 4.8 The indirect bandgap,  $E_{g(i)}$ , can be estimated from the and  $(\alpha h\nu)^{1/2}$  versus  $h\nu$  plot. Generally, EDOT and derived PEDOT show a direct bandgap [36]. So, in this study, values of direct bandgap  $E_{g(d)}$  of the PPEDOT thin films were estimated, which are presented in Table 4.3.

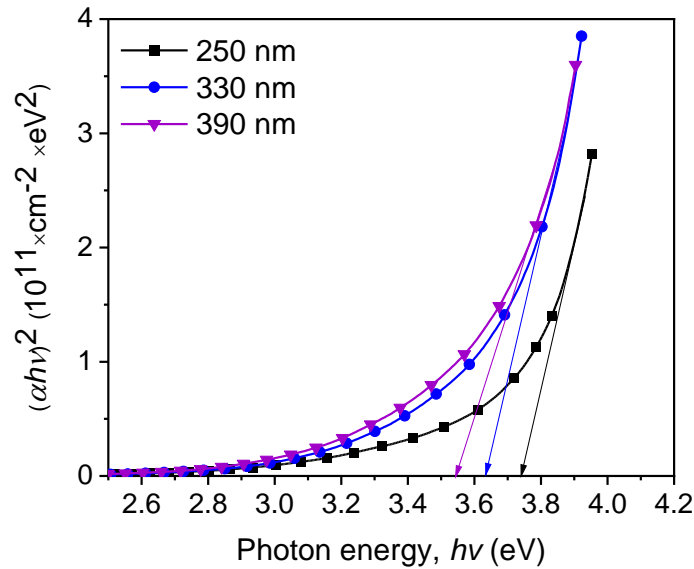


**Fig. 4.8** Band gap energy of PPEDOT thin films using the Tauc relation of different thicknesses.

**Table 4.3** Bandgap and  $\lambda_{max}$  values of PPEDOT thin films of different thicknesses.

Deposition time (min)	Thickness, $d$ (nm)	$\lambda_{max}$ (nm)	$E_g$ (eV)
30	250	266	3.75
45	330	272	3.63
60	390	277	3.54

$E_g$  reduces significantly with increasing thickness because some crosslinking may happen inside the bulk of the material because of the influence of plasma on the surface during the deposition process.

The Urbach energy,  $E_u$ , is one of the most significant optical characteristics that indicates defect states or disorders in thin films. The defect states in the optical band edge area that cause the absorption tail to appear in the absorption spectra are represented by  $E_u$ . Urbach spectral tail is the name given to the absorption tail, while Urbach energy is the name given to the energy associated with it ( $E_u$ ). The Urbach empirical rule that characterizes the spectrum dependence of  $h\nu$  in the low photon energy zone is provided by the following equation [66].

$$\alpha = \alpha_0 \exp\left(\frac{E}{E_u}\right) \quad (4.3)$$

Here,  $E_u$  is the incident photon energy and  $\alpha_0$  is a constant. A straight-line equation can be obtained taking the logarithm on both sides of the Eq. 4.3.

$$\ln\alpha = \ln\alpha_0 + \frac{E}{E_u} \quad (4.4)$$

The value of  $E_u$  is calculated from the inverse gradients of the graphs  $\ln\alpha$  versus  $h\nu$  plots which are represented in Fig. 4.9 for the as-deposited PPEDOT thin films provide.

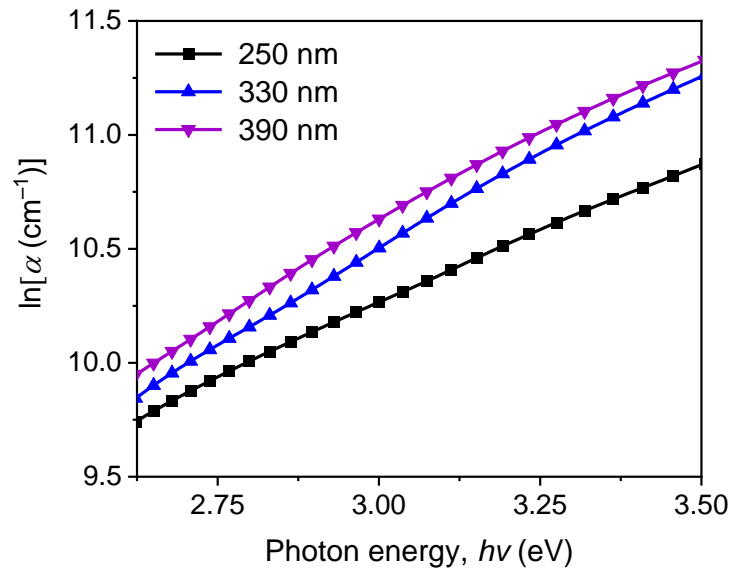


**Fig. 4.9** The  $\ln\alpha$  vs  $h\nu$  plots for thickness dependent PPEDOT (AC) films.

The calculated  $E_u$  values have been presented in Table 4.5 and the significant about  $E_u$  values that it decreases with increasing film thickness. It may occur due to the decrease

of defects in the PPEDOT films [66] and indicate less structural disorder in the introduction of localized states within the forbidden energy bandgap.

The correlated parameter with  $E_u$  known steepness parameter,  $\sigma_s$ , can be estimated using the following relation to study the broadening of the optical absorption edge in consequence of electron-phonon or exciting-phonon interactions [60],

$$\sigma_s = \frac{k_B T}{E_u} \quad (4.5)$$

Here,  $k_B$  is the Boltzmann constant and  $T$  being the absolute temperature. The  $\sigma_s$  values are determined by taking  $T = 298$  K and are listed in Table 4.4 and it is seen that  $\sigma_s$  value of is increasing with increases of thicknesses.

**Table 4.4** Variation of  $E_u$  and  $\sigma_s$  of as-deposited PPEDOT thin films.

PPEDOT Films	Urbach energy, $E_u$ (eV)	Steepness parameter, $\sigma_s$
250 nm	0.78	0.033
330 nm	0.61	0.039
390 nm	0.56	0.046

The extinction coefficient ( $k$ ) curve is calculated using Eq. 4.6. The value of  $k$  expresses the attenuation of light beam in a medium and it is important optical parameter associated with the absorption. The plot of extinction coefficient with wavelength for the thickness dependent PPEDOT thin films is displayed in Fig. 4.10.

$$k = \frac{\alpha \lambda}{4\pi} \quad (4.6)$$

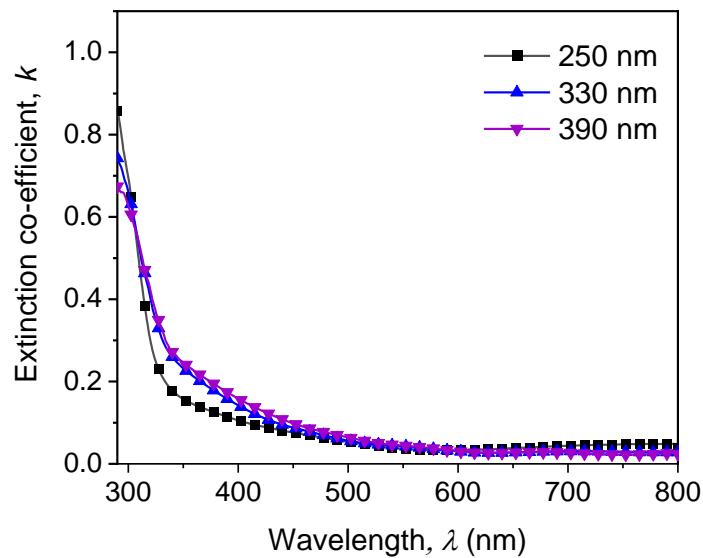


**Fig. 4.10** The variation of extinction coefficient,  $k$  with  $\lambda$  for as-deposited PPEDOT (AC) films.

It is noticed that the  $k$  value drops with increasing wavelength, suggesting that electron transport across the mobility gap with  $\lambda$  [61].

The refractive index of a material,  $\mu$ , is used to measure how light propagates through a material. The  $\mu$  value greater than 1.5 is consider as high polymer. The higher value of  $\mu$  indicates slower velocity of electromagnetic waves through the materials. Using the Fresnel's formula (Eq. 4.7), the values of  $\mu$  are measured [60] and the variation of  $\mu$  against wavelength  $\lambda$  is plotted in Fig. 4.11.

$$\mu = \left( \frac{1+R}{1-R} \right) + \sqrt{\frac{4R}{(1-R)^2} - k^2} \quad (4.7)$$

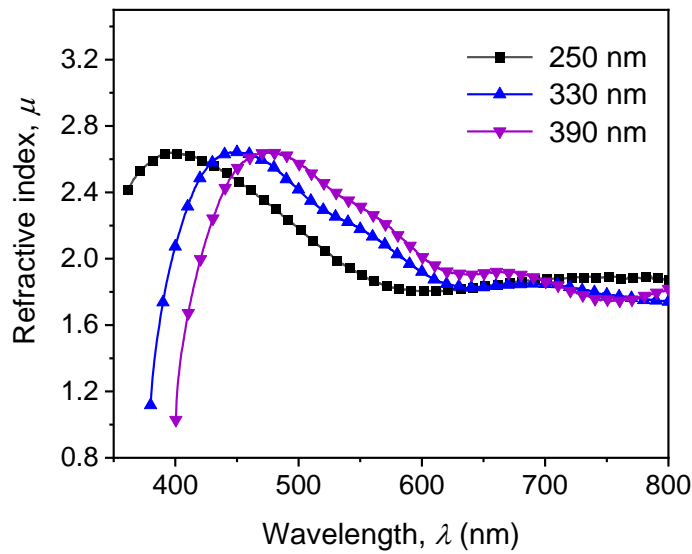


**Fig. 4.11** The refractive index plots against  $\lambda$  for as-deposited PPEDOT (AC) thin films.

It is pointed out that the  $\mu$  values for all samples reach as high as 2.64 corresponding 400 nm wavelength region. Nevertheless,  $\mu$  values slightly change with variation of power source, which indicates the increase in interactions taking place between the photons and electrons of the films.

Again, the optical response of the deposited thin films can be understood with the help of optical conductivity ( $\sigma_{opt}$ ). The variation of  $\sigma_{opt}$  with wavelength for different thicknesses of the films can be calculated by using the following equation [62],

$$\sigma_{opt} = \frac{\omega n c}{4\pi} \quad (4.8)$$

Where,  $c$  is the velocity of light. The changes in  $\sigma_{opt}$  are plotted against  $\lambda$  and are presented in Fig. 4.12. The maximum value of  $\sigma_{opt}$  is noted at lower wavelength

regions (345 to 450 nm). The value of  $\sigma_{opt}$  the samples approach zero at higher wavelengths (above 600 nm) for all the deposited PPEDOT thin films.

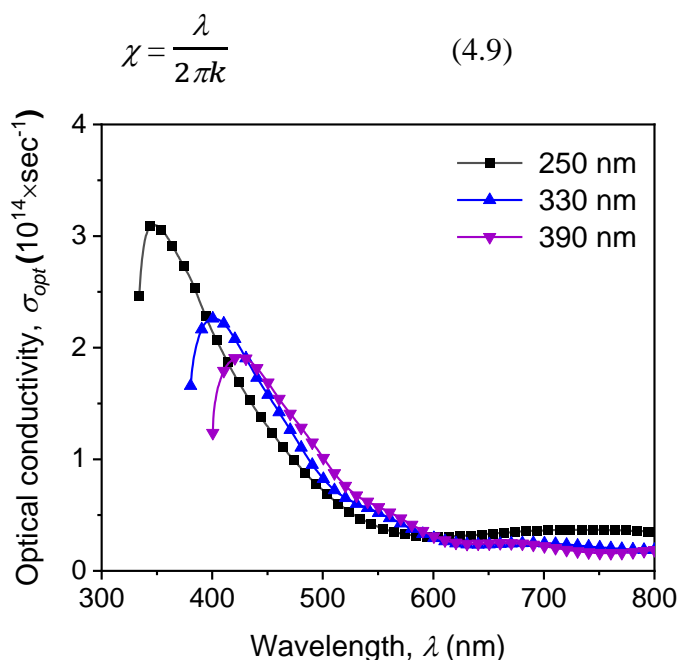


**Fig. 4.12** The optical conductivity ( $\sigma_{opt}$ ) with wavelength of thickness dependent PPEDOT (AC) films.

The interaction between an incident wave of light and the electron in the material is determined by the size of the skin depth. The depth at which the amplitude of an electromagnetic wave is lowered by a factor of  $1/e$  is known as skin depth ( $\chi$ ) which is calculated using the following the relationship [63].

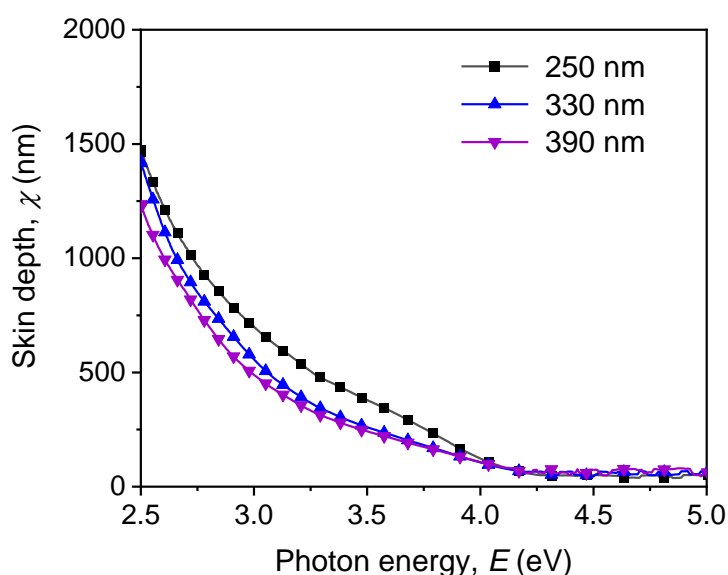


**Fig. 4.13** The variation of skin depth ( $\chi$ ) against photon energy for the as-deposited thickness dependent PPEDOT (AC) films.

Fig. 4.13 depicts the relationship between skin depth and energy. It has been discovered that  $\chi$  lowers monotonically with increasing photon energy and broadens with diverse film power sources. At greater energy levels, the skin depth steadily decreases. It might happen because of increased electron collisions causing energy loss.

#### **4.4 Thermal Analyses: TG/DSC of AC PPEDOT films**

The TG and DSC analyses have been carried out to characterize the decomposition and the thermal stability of the PPEDOT thin films. The TG and DSC traces taken for AC and RF plasma polymer at a heating rate of 10 K/min in nitrogen atmosphere in the temperature range of 298 – 873 K.

The thickness dependent TG/DSC curves for AC PPEDOT powder samples taken in nitrogen atmosphere are shown in Fig. 4.14. Different phases of mass loss owing to heating are shown by the TGA trace of PPEDOT (AC) films presented in Fig. 4.14 (a).

Weight losses at various region based on applied temperature to PPEDOT have been recorded as A, B, and C as shown in Table 4.5. In A region, from 298 K to 415 K temperature, lower weight losses are recorded like 0.81 (wt%), 0.48 (wt%) and 0.33 (wt%) with the thicknesses of film 250 nm, 330 nm, and 390 nm, respectively. In B and C region, weight losses are increased with increasing thickness.

At 755 K temperature, the PPEDOT thickness of 250 nm, 330 nm and 390 nm remained 91 (wt%), 89 (wt%) and 87 (wt%) weight, respectively. The weight loss in the low temperature region of A, up to around 298 - 415 K, may be attributable to the removal of absorbed surface water, in region B, the weight loss may be due to the removal of some unreacted monomer, or it could be unrelated to any changes in the PPEDOT structure. In region (A) and (B), weight reduction for all samples is minimal, around 0.33 - 1.54 (wt%). After 495 K, there is a significant weight loss, which might be due to thermal degradation or a breakdown response [35].

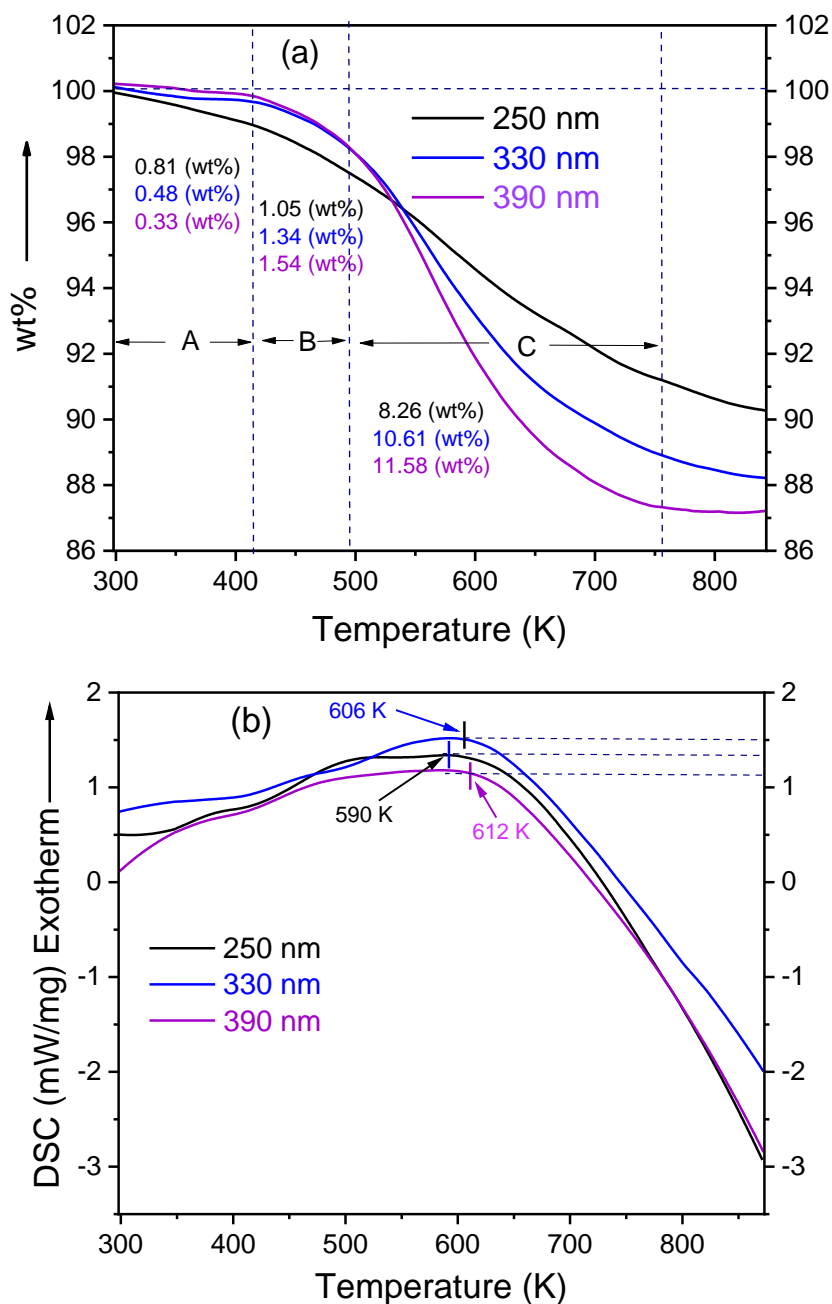


**Fig. 4.14** Thermograms of (a) TGA; (b) DSC of thickness dependent PPEDOT thin films in  $N_2$  environment at scanning rate of 10 K/min.

The DSC thermogram as shown in Fig. 4.14 (b) reveals exothermic wide band that peaks about 590 K, 606 K and 612 K for the sample of 250 nm, 330 nm and 390 nm thicknesses, respectively. It suggests that the rate of mass loss is increasing. As a result, PPEDOT (AC) films are thermally stable up to around 612 K.

**Table 4.5** The weight loss (wt %) and stability temperature of PPEDOT (AC) thin films.

Region	Temperature (K)	Weight loss (wt %) of PPEDOT (AC) thin films		
		250 nm	330 nm	390 nm
A	298 – 415	0.81	0.48	0.33
B	415 – 495	1.05	1.34	1.54
C	495 – 755	8.26	10.61	11.58
Stability temperature (K)		590	606	612

#### 4.5 DC Electrical Properties of Plasma Polymerized PPEDOT (AC) Thin Films

Various carrier transport mechanisms in insulating polymer thin films based on the dependence of current density ( $J$ ) on voltage ( $V$ ), temperature ( $T$ ), and thickness ( $d$ ) have been suggested. To determine the predominance of a certain mechanism, the dependency of the current density on the described parameters needs to be analyzed.

Generally polymeric material changes its behavior from insulating properties to electrical properties when an electrical field is applied to them and charges in the polymer are redistribute if they are mobile enough to respond in the time scale of the applied field. The  $J$ - $V$  characteristics follow a power law of the form  $J \propto V^n$ , where  $n$  is a power index [65], with variable values of ‘ $n$ ’ (slope). Two conduction mechanisms are found in polymer thin film, like Ohmic and non-Ohmic, when  $n$  is unity, the conduction is Ohmic and the value of  $n$  is less or more than unity, then the conduction process is not Ohmic. Ohmic conduction is found in lower voltage region and non-Ohmic Ohmic conduction is found in the upper voltage region. Thermal or Schottky effect, space-charge-limited conduction (SCLC), and Poole-Frenkel (PF) conduction are the three most likely mechanism processes identified in polymer thin films [48, 49].

##### 4.5.1 Current density-voltage ( $J$ - $V$ ) characteristics

A typical  $J$ - $V$  characteristic curves for PPEDOT (AC) thin films with thicknesses of 250, 330, and 390 nm observed at various temperatures in the voltage range of 0.3 V to 100 V are shown Fig. 4.15 (a), (b) and (c), respectively. At room temperature,  $J$ - $V$  plot for different thicknesses is shown in Fig. 4.15 (d). The current density rises with



increasing voltage and temperature, as seen in the graph. The curves are nearly identical in form, with two parts in the low and high voltage areas with distinct slopes, implying two separate conduction mechanisms. The values of  $n$  are calculated for all the samples at different temperature and are presented in Table 4.6.

In the low voltage region ( $< 15\text{V}$ ), the value of slopes ( $n$ ) lies in between  $0.13 \leq n \leq 0.81$  indicating Ohmic conduction mechanism whereas in the high voltage region ( $>15\text{ V}$ ), the slope of the graph is found to lie in  $1.03 \leq n \leq 3.15$ , indicating a non-Ohmic conduction mechanism. In the higher voltage region, the three main transport mechanisms typically observed in organic polymer thin films are Richardson-Schottky (RS) conduction, Poole-Frenkel (PF) conduction, and space-charge-limited conduction (SCLC) [64, 65].

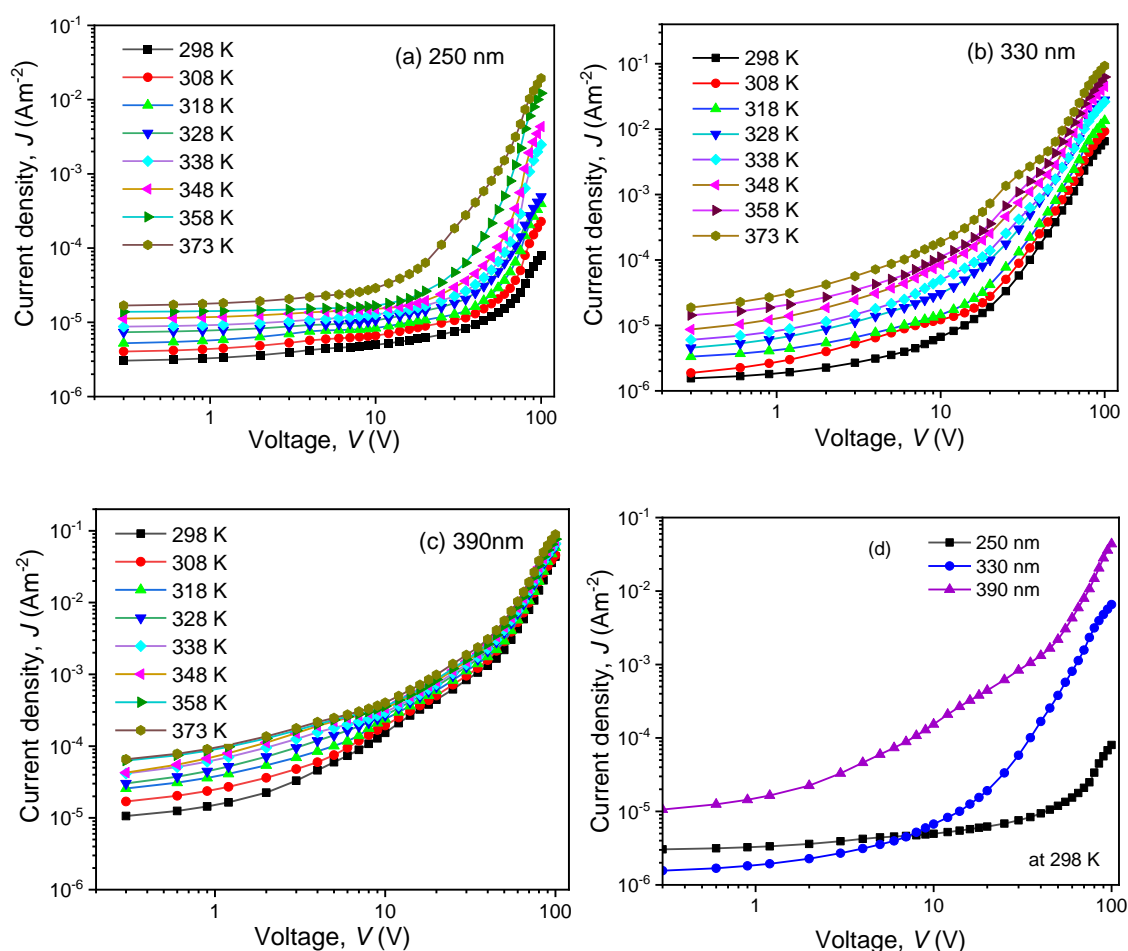


**Fig. 4.15**  $J$ - $V$  relationship for PPEDOT (AC) films of thickness (a) 250 nm, (b) 330 nm and (c) 390 nm at different temperatures, (d) for the film at room temperature (298 K).

**Table 4.6** The slopes in the lower and higher voltage regions at different temperatures for PPEDOT (AC) thin films of different thicknesses.

Thickness, $d$ (nm)	Measurement temperature (K)	Value of slopes, $n$	
		Low voltage region ( $< 15V$ ) (Ohmic)	High voltage region ( $> 15V$ ) (non-Ohmic)
250	298	0.17	1.03
	308	0.18	1.11
	318	0.17	2.73
	328	0.19	2.33
	338	0.14	2.98
	348	0.17	3.03
	358	0.21	3.12
	373	0.13	3.15
330	298	0.44	2.91
	308	0.51	2.74
	318	0.43	2.93
	328	0.61	2.84
	338	0.67	2.77
	348	0.57	2.91
	358	0.63	2.81
	373	0.68	2.78
390	298	0.77	2.54
	308	0.71	2.47
	318	0.62	2.79
	328	0.58	2.57
	338	0.73	2.47
	348	0.59	2.42
	358	0.71	2.36
	373	0.81	2.28

The dependence of  $J$  on  $d$  obeys the relation  $J \propto d^l$ , where  $l$  is a parameter depends on the presence of traps in the films. The absolute value of  $l \geq 3$  indicates the SCLC mechanism, while  $l < 3$  for Schottky or PF conduction mechanism. To study the actual

conduction mechanism,  $J$  is plotted against  $d$ , for PPEDOT thin films of different thickness in the non-Ohmic region at 60 V which is presented in Fig. 4.16.

The linear slope derived from Fig. 4.16 gives a negative value of 5.48, which is much higher compared to the value considered for RS or PE conduction. So, this observation does not signify the possibility of presence of RS or PF mechanism in the PPEDOT thin films. Therefore, it may have inferred that the conduction mechanism operative in these films is SCLC [66].

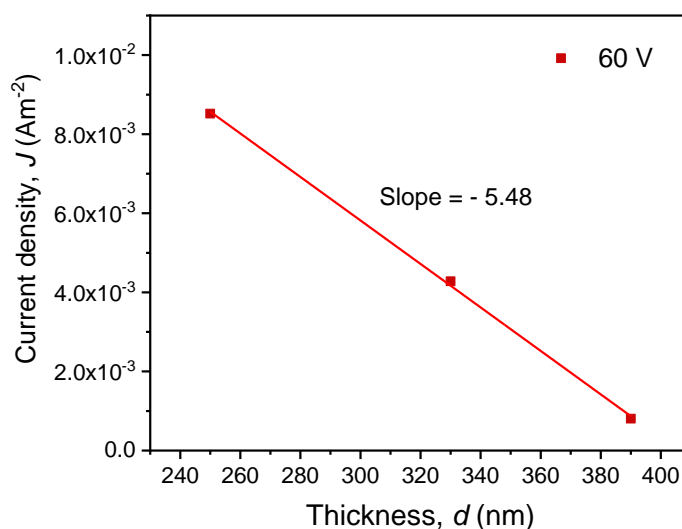


**Fig. 4.16** Plots of  $J$  vs  $d$  for PPEDOT (AC) thin films in the non-Ohmic region (at voltage 60 V).

#### 4.5.2 Dependence of $J$ on temperature

The temperature dependency of the current density,  $J$ , is investigated using the Arrhenius equation. The Arrhenius equation can be expressed as

$$J = J_0 \exp\left(-\frac{\Delta E}{k_B T}\right) \dots\dots\dots (4.10)$$

Where,  $J_0$  is the current density at the thermal equilibrium,  $\Delta E$  is the activation energy and  $k_B$  are the Boltzmann constant. The dependence of  $J$  on  $1/T$  for PPEDOT (AC) thin films of different thicknesses are shown in Fig. 4.17 (a-b).

From  $J$ - $V$  characteristics, it is found that two types of conduction mechanisms (Ohmic and non-Ohmic) would be present in this PPEDOT films. In lower voltage region up to  $\sim 10$  V, the slopes of  $J$ - $V$  graphs follow straight line. The slopes remain similar at any points of Ohmic region. From this view, the  $\Delta E$  in the Ohmic region is determined at 5 V. Again, after 10 V,  $J$ - $V$  characteristics follow the power law, where maximum

changes of current density have been changed around 60 V. That's why, the  $\Delta E$  are evaluated from the slopes of  $J$  versus  $1/T$  curves in these two voltage regions: on at the higher ( $V = 60$  V) and other at the lower ( $V = 5$  V) voltages and are documented in Table 4.7. At an applied voltage of 5 V, the  $\Delta E$  are found to be around an average value of 0.076 eV in Ohmic region whereas, in the non-Ohmic region  $\Delta E$  were found to be around 0.119 eV for an applied voltage of 60 V.

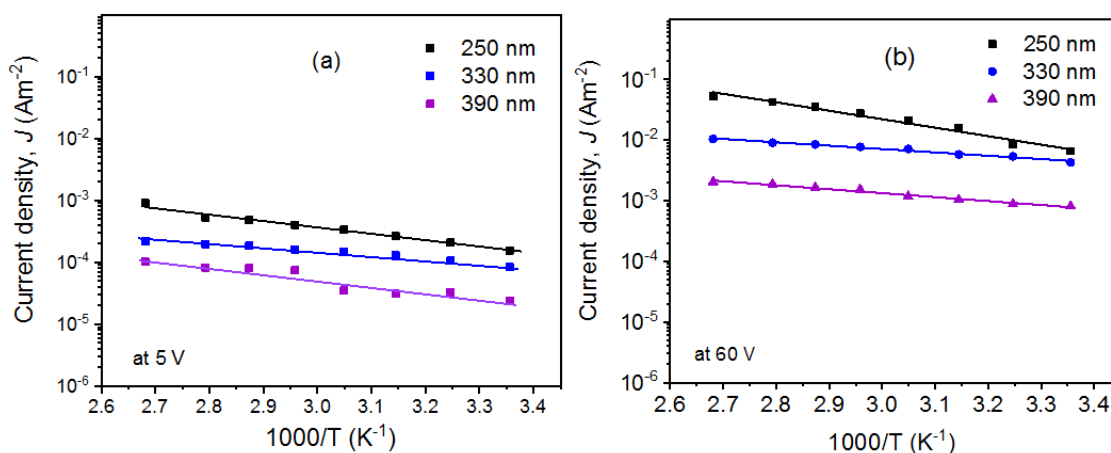


**Fig. 4.17** Variation of  $J$  with  $1/T$  for PPEDOT (AC) thin films of thicknesses 250 nm, 330 nm, and 390 nm at (a) 5 V (Ohmic) and (b) 60 V (non-Ohmic) regions.

**Table 4.7** Values of activation energy  $\Delta E$  (eV) for PPEDOT (AC) thin films of different thicknesses.

Thickness, $d$ (nm)	Activation energies, $\Delta E$ (eV)	
	5 V (Ohmic)	60 V (non-Ohmic)
250	0.066	0.108
330	0.074	0.118
390	0.089	0.131

In the Ohmic and non-Ohmic regions, low  $\Delta E$  suggests that the thermally activated hopping conduction is operational in these films. A shift from hopping regime to a regime with distinct energy levels might be linked to the change from lower to higher values in  $\Delta E$  in the high temperature regions [66].

#### 4.6 Morphological, Structural, Thermal, Optical and DC Electrical Properties of PPEDOT (AC) Thin Films and Previous Works

The properties such as morphological, structural, optical, thermal, and electrical acquired from various experimental investigations in PPEDOT (AC) thin films and previous work are noted in Table 4.8.

**Table 4.8** Various properties of as-deposited PPEDOT (AC) thin films and previous work.

Property	PPEDOT (AC) thin films	Previous work
Surface morphology	Smooth and pinhole free	Three-dimensional network-like structure [26]
Elemental constituent	Pure	Pure [28]
Structural behavior	Crosslinked	Crosslinked
Band gap energy	3.75 - 3.54 eV	4.122 eV [31]
Thermal stability	Stable up to 590 - 612 K	Stable up to 510 K [35]
Conduction mechanism	SCLC	SCLC [33]
Activation energy	0.076 eV in Ohmic, and 0.119 eV in non-Ohmic region	0.43 eV [33]

#### 4.7 Comparative Study Among Various Characteristics of PPEDOT (AC) and PPEDOT (RF) Thin Films

To compare AC and RF PPEDOT thin films, a thin film was prepared using RF plasma and its morphological, elemental, structural, optical, thermal and electrical measurements were determined by same procedure as prepared the PPEDOT (AC) thin film at the thickness of 250 nm whereas RF samples show 690 nm thickness.

##### 4.7.1 FESEM study

The PPEDOT (AC) thin films of thicknesses 250 nm with different magnifications as  $\times 50$  k,  $\times 100$  k is displayed in Figs. 4.18 (a) and (c), respectively, and the PPEDOT (RF) thin films of thicknesses 690 nm prepared by radio frequency power source with different magnifications as  $\times 50$  k,  $\times 100$  k is displayed in Figs. 4.18 (b) and (d), respectively. Though input power influences the degree of polymerization, there are no significant changes that can be found between PPEDOT (AC) and PPEDOT (RF) thin films. Finally, it can be said that the surfaces of both films are also smooth, pinhole-

free, scratch-less, flawless, and homogeneous at all magnifications as-followed by AC films.

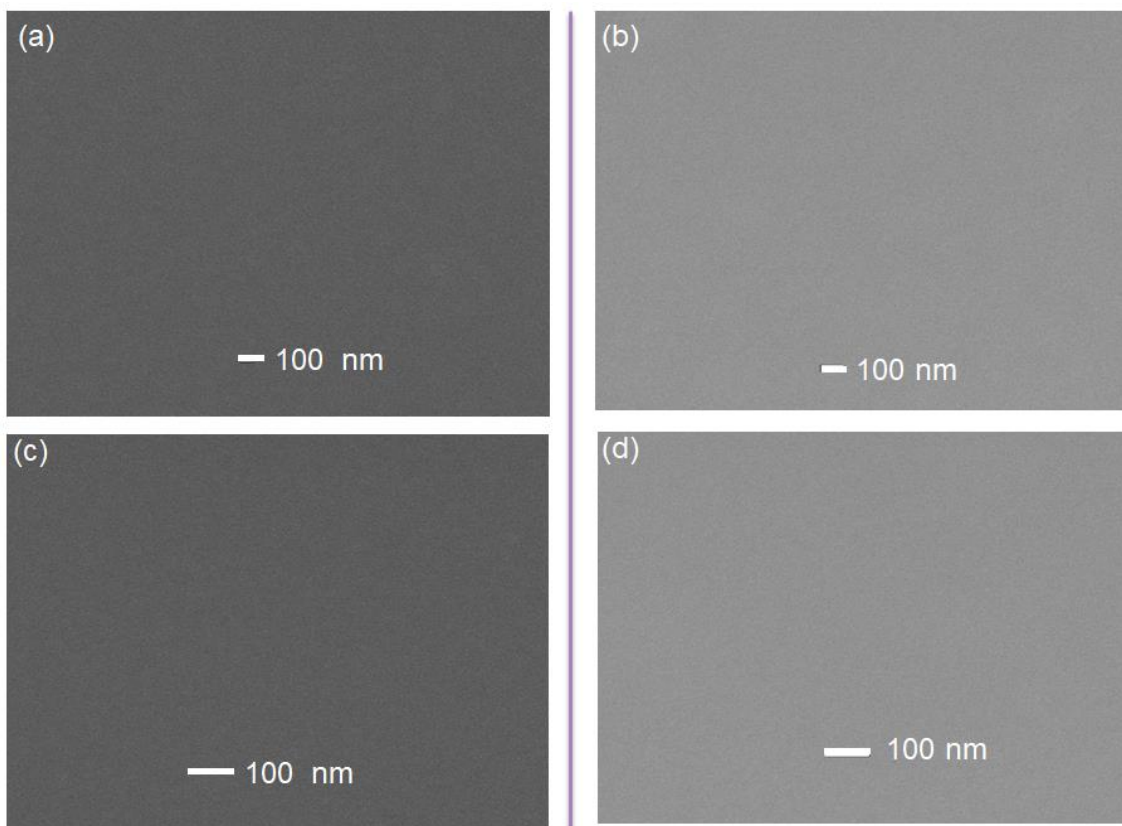


**Fig. 4.18** Comparison of FESEM surface morphology images as deposited (a)  $\times 50$  k, (c)  $\times 100$  k for PPEDOT (AC), and (b)  $\times 50$  k, (d)  $\times 100$  k for PPEDOT (RF) films.

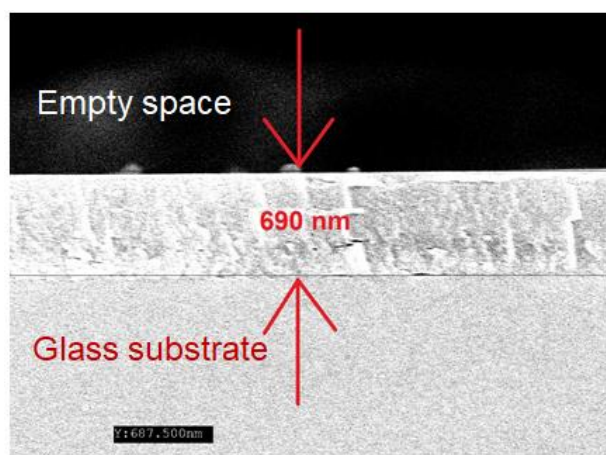


**Fig. 4.19** Cross-sectional view PPEDOT (RF) of thickness 690 nm.

A cross sectional image of an as-deposited PPEDOT (RF) thin film with a thickness of 690 nm by FESEM is shown Fig. 4.19. Additionally, it can be mentioned here that the

thickness of PPEDOT (RF) film is calculated about 660 nm using multiple-beam interferometer and about 4.5% error findings of thickness are noted in these two-measurement techniques. Meanwhile, the prepared PPEDOT (RF) thin films onto glass substrates are deposited uniformly and no substantial grain is visible in the cross-sectional image.

#### 4.7.2 EDX analyses

The EDX spectra of the as-deposited PPEDOT thin films are shown in Fig. 4.20 for the films fabricated by AC and RF plasma polymerization technique, respectively.

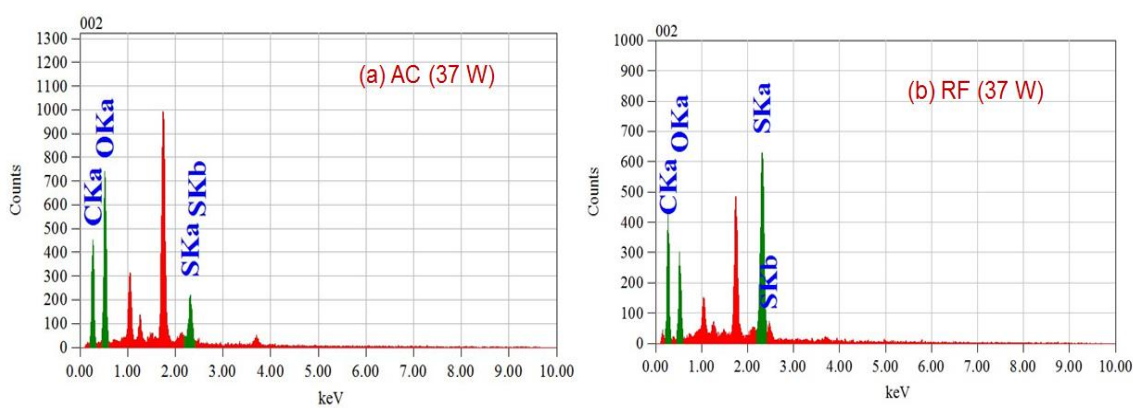


**Fig. 4.20** EDX spectra of (a) AC (37 W) and, (b) RF (37 W) of PPEDOT thin films.

**Table 4.9** Atomic percentage (at%) of the elements present in the PPEDOT thin films.

Element detected	Elements in PPEDOT (at%)	
	AC sample	RF sample
	250 nm	690 nm
C	51.51	69.40
O	44.36	19.70
S	4.13	10.90
H	Not detected	Not detected
Total	100.00	100.00

The atomic percentage (at%) of constituent elements the of PPEDOT thin films are listed in Table 4.9. The (at%) of C and S in the RF samples are greater than AC samples. It may happen due to higher thickness of the RF samples or the probable loss of H and O throughout the time of plasma polymerization [32].

#### 4.7.3 Structural Analyses: FTIR Spectroscopy

The FTIR spectra of AC and RF PPEDOT thin films at room temperature are presented in transmittance mode ranging from 3500 to 500  $\text{cm}^{-1}$  wavenumber as shown in Fig. 4.21. The RF PPEDOT contains more broader spectrum than AC PPEDOT assigned from 760 to 1708  $\text{cm}^{-1}$ , which corresponds to different significant modes. The absorption peaks around 2929  $\text{cm}^{-1}$  for AC (37 W) and 2915  $\text{cm}^{-1}$  for RF (37 W) has come from the monomer absorption peak 2934 corresponding C-H symmetric stretching vibrations.

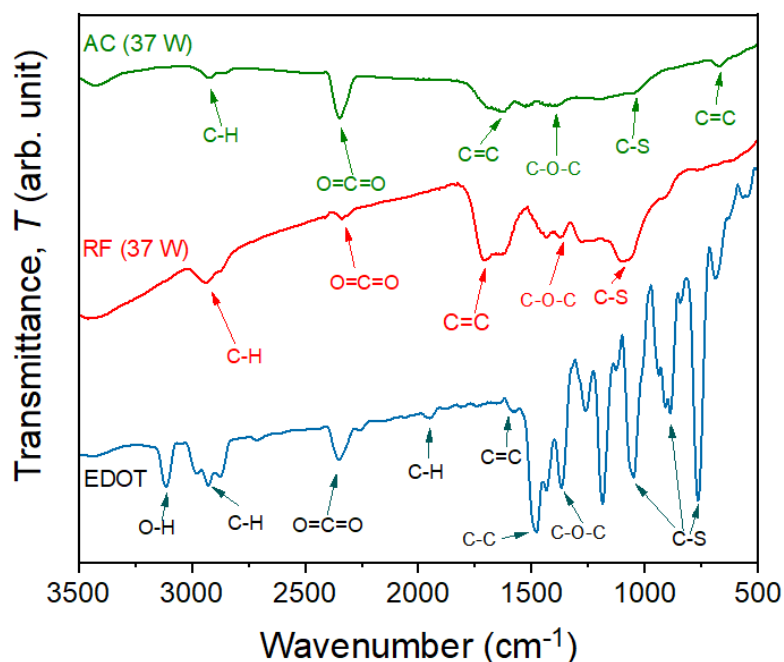


**Fig. 4.21** FTIR spectra as-deposited AC (37 W) and RF (37 W) PPEDOT thin films.

The stretching absorption band  $\text{O}=\text{C}=\text{O}$  has shifted slightly to lower wavenumber appearing to 2336  $\text{cm}^{-1}$ . A strong absorption band  $\text{C}=\text{C}$  has created corresponding to 1708  $\text{cm}^{-1}$  in RF PPEDOT films indicates the presence of conjugation i.e.,  $\text{C}=\text{C}$  stretching vibrations. The presence of  $\text{C}-\text{O}-\text{C}$  stretching vibrations modes in ethylenedioxy groups has confirmed by the absorption peaks around 1365 and 1377  $\text{cm}^{-1}$ .

Additionally, the  $\text{C}-\text{S}$  of thiophene backbone is also presented at the sharp absorption peak at about 1085-760  $\text{cm}^{-1}$ , which is attributed to  $\text{C}-\text{S}$  ring vibration disappear in the PPEDOT spectra [31].



**Table 4.10** The FTIR spectroscopic assignments of the AC and RF PPEDOT thin films.

Assignment	Wavenumber (cm <sup>-1</sup> )		
	Monomer EDOT	PPEDOT thin films	
		AC (37 W)	RF (37 W)
O-H stretching	3113	----	----
C-H stretching	2934	2926	2915
O=C=O stretching	2357	2343	2336
C-H bending	1951	----	----
C=C stretching	1584	1620	1708
C-C stretching	1471	----	----
C-O-C	1365	1377	1365
C-S ring stretching	1053, 890, 760	1045	1085
C-H	661	662	670

Though, both samples show almost similar spectra corresponding with O-H stretching, C-H stretching, O=C=O stretching, C=C, C-C, C-S, and out of plane bending, but all the peaks have shifted slightly as a function of wavenumber in the AC and RF PPEDOT spectra which suggest that the chemical structure is modified due to different power sources.

#### 4.7.4 UV-Visible Spectroscopic Analyses

Several optical parameters including absorbance, transmittance, absorption co-efficient, optical band gap, Urbach energy, steepness parameter, extinction co-efficient, refractive index, optical conductivity, and skin depth was investigated to compare between AC and RF PPEDOT thin films. These optical spectra were performed in the wavelength range of 200 nm to 800 nm at room temperature. Fig. 4.22 shows the variation of absorbance and transmittance corresponding AC and RF PPEDOT thin films.

It is noticed that all absorption peaks for AC and RF films appeared in the UV region where the maximum wavelength values for all peak's absorbance transferred slightly to the lower wavelength as mentioned in Table 4.11. It may be assigned to the persistence of conjugation in thin film [58]. It is also observed that the intensity of the absorption

peak does not change significantly, and the absorbance of all the films becomes almost zero in the visible region.

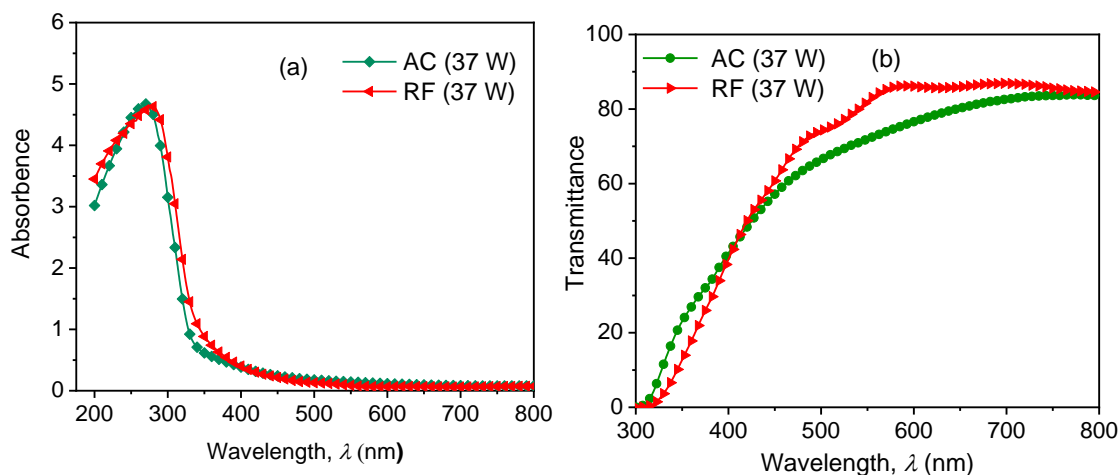


**Fig. 4.22** (a) Spectral distribution of (a) absorbance, (b) transmittance of AC (37 W) and RF (37 W) PPEDOT films as a function of wavelength.

Meanwhile, in the lower wavelength region, the RF sample shows slightly low transmittance to AC samples, but it shifts quickly to 86% transmittance at  $\sim 575 - 735$  nm. Otherwise, no significant changes are observed in this wavelength region. That's why, it can be confirmed that all the films are transparent in the visible region.

The absorption coefficient of AC and RF PPEDOT thin films is displayed in Fig. 4.23 (a) using Eq. 4.1.

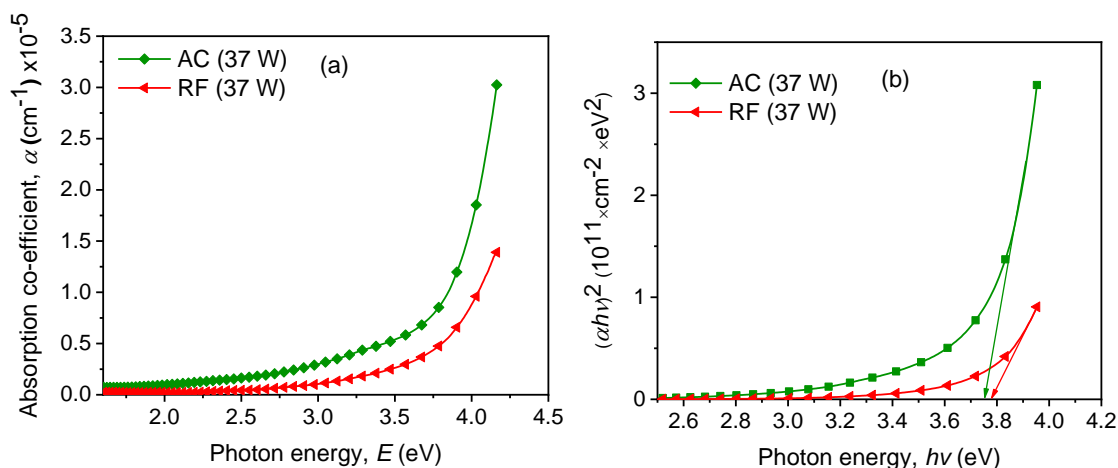


**Fig. 4.23** (a) Plot of absorption coefficient,  $\alpha$  with  $h\nu$ , (b) band gap energy using the Tauc relation, for PPEDOT thin films of different plasma power.

The absorption rate of AC film is higher than that of RF samples, that may happen due to different optical transitions in the PPEDOT thin films. Fig. 4.23 (b) shows the optical

band gap,  $E_g$ , whereas the RF sample exhibits the highest optical bandgap as calculated of  $\sim 3.77$  eV, because some crosslinking may be developed within the bulk of the material owing to the impact of plasma on the film surface during the deposition process.

**Table 4.11** Bandgap and  $\lambda_{max}$  values of PPEDOT thin films of different thicknesses.

Deposition time (min)	Thickness, $d$ (nm)	$\lambda_{max}$ (nm)	$E_g$ (eV)
30 (AC)	250	266	3.75
30 (RF)	690	268	3.77

The Urbach energy,  $E_u$ , is calculated from the Eq. 4.2 for AC and RF samples which are represented in Fig. 4.24 (a). The obtained  $E_u$  values, noted in Table 4.12 shows that the values of  $E_u$  change slightly between AC and RF PPEDOT thin films, which might have occurred due to the increase of disorder in the films and also suggests the introduction of localized states within the forbidden energy bandgap [59].

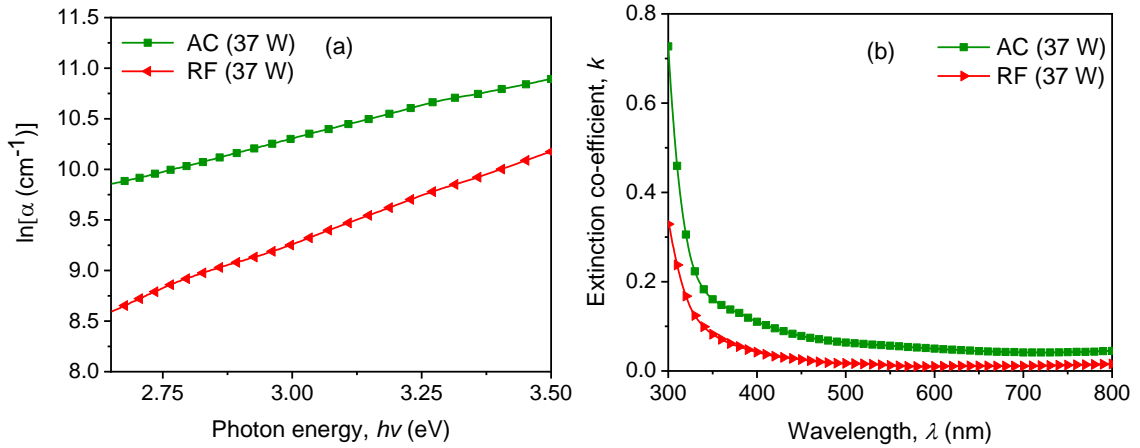


**Fig. 4.24** (a) The  $\ln\alpha$  vs  $h\nu$  plots, (b) extinction coefficient,  $k$  with  $\lambda$ , for AC and RF PPEDOT thin films.

**Table 4.12** Variation of  $E_u$  and  $\sigma_s$  of as-deposited PPEDOT thin films.

PPEDOT Films	Urbach energy, $E_u$ (eV)	Steepness parameter, $\sigma_s$
AC	0.78	0.033
RF	0.88	0.029

The steepness parameter,  $\sigma_s$  values are determined by correlated parameter of  $E_u$ , which are listed in Table 4.12, and it is seen that  $\sigma_s$  value of RF film is slightly lower than that of AC films. Fig. 4.24 (b) shows the comparison of extinction coefficient ( $k$ ) between

AC and RF films where AC sample is always higher compared to RF samples, which indicating the possibility of a decrease in electron transfer across the mobility gap with  $\lambda$  [61].

Comparison of refractive index, optical conductivity and skin depth between AC and RF films are presented in the following figures. The refractive index value,  $\mu$ , values slightly change with variation of power source (AC and RF) which indicates the increase in interactions taking place between the photons and electrons of the films as shown in Fig. 4.25 (a). Again, the optical response of the deposited AC and RF PPEDOT films can be understood with the help of optical conductivity ( $\sigma_{opt}$ ), which is described in Fig. 4.25 (b). It is clearly seen that  $\sigma_{opt}$  AC films are higher than that of RF films.

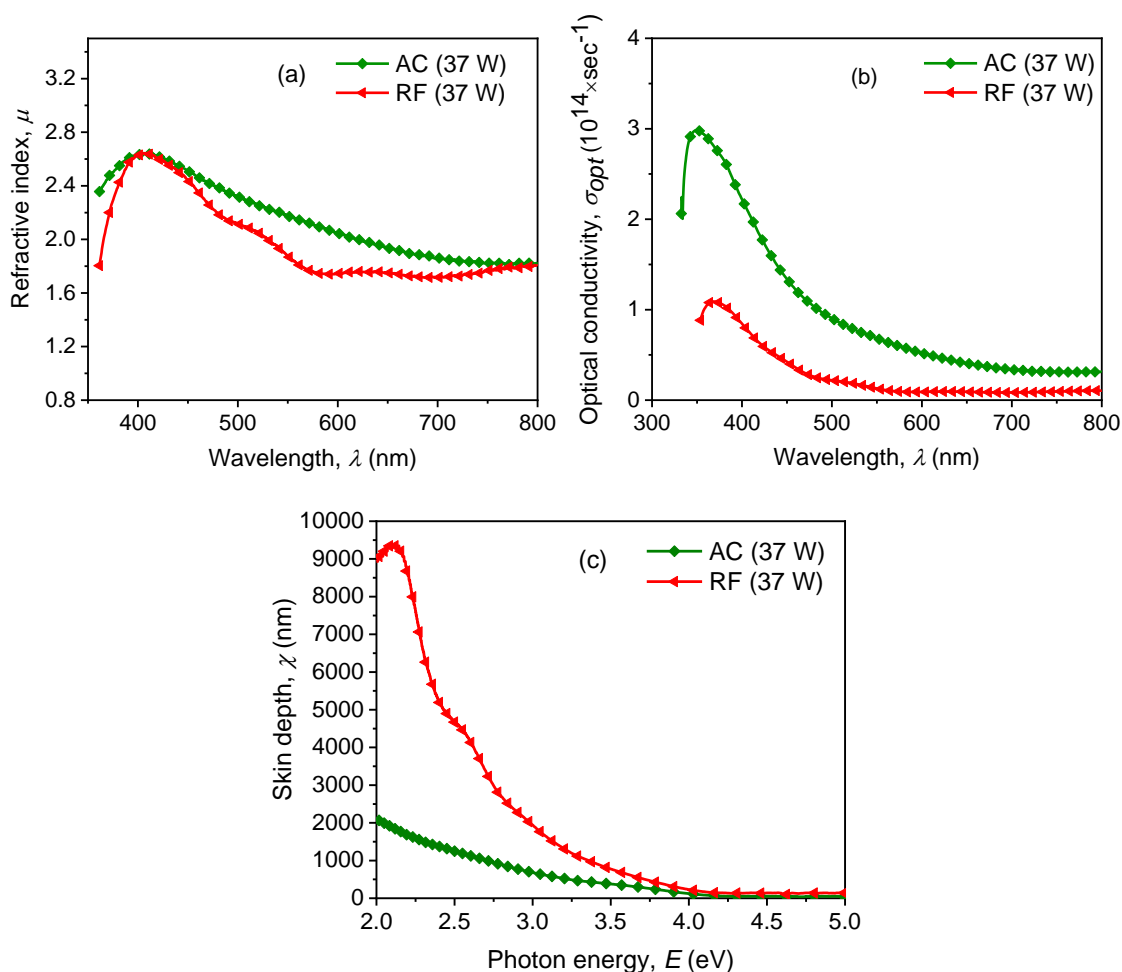


**Fig. 4.25** (a) The refractive index plot against  $\lambda$ , (b) the optical conductivity ( $\sigma_{opt}$ ) with wavelength and, (c) the skin depth ( $\chi$ ) against photon energy, for AC and RF PPEDOT thin films.

The skin depth ( $\chi$ ) measures the contact between an incident wave of light and the electron in the AC and RF PPEDOT thin films. It has been seen in Fig. 4.25 (c) that AC sample shows smaller value of  $\chi$  than that of RF samples which indicates the lowers monotonically with increasing photon energy and broadens with diverse film power sources. At greater energy levels, the skin depth steadily decreases. It may be happened because of increased electron collisions causing energy loss.

#### 4.7.5 TG/DSC of RF PPEDOT films

The TGA trace of AC (37) and RF (37 W) thin films has been also taken from 298 to 843 K and showed different stages of thermal decomposition owing to heating, which divided in three regions as shown in Fig. 4.26 (a).

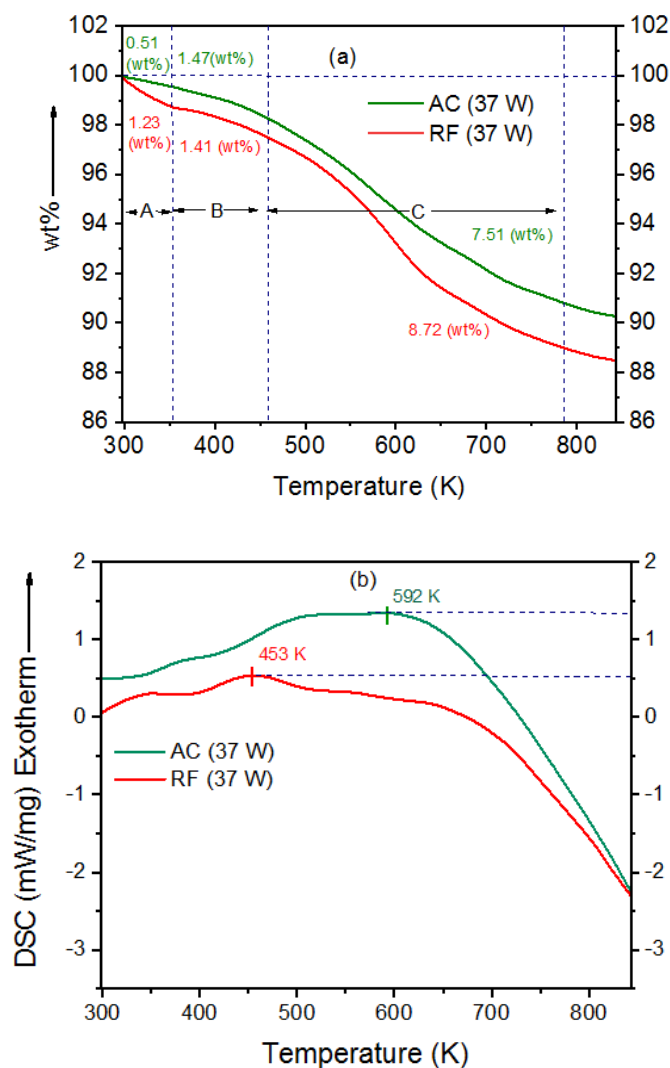


**Fig. 4.26** (a) Weight loss (wt%) and (b) DSC of PPEDOT thin films in nitrogen atmosphere at scanning rate of 10 K/min.

Though weight loss of RF sample is greater than that of AC samples, but every region may be associated with a different rate of weight loss. In region A, the weight loss about 0.51 (wt%) for AC samples and 1.23 (wt%) for RF samples respectively, may be due to the loss of absorbed moisture in the PPEDOT films. After that weight loss in B region 1.47 (wt%) for AC samples and 1.41 (wt%) for RF samples are detected which may be happened due to the removal of some unreacted monomer.

In region C, after 460 K temperature, a huge weight loss occurred may be due to the thermal decomposition/ or breakdown reaction. The weight losses of AC samples in this region are 7.51 (wt%) and finally it holds 90.19 (wt%) weight as residue. Meanwhile, after failing 8.72 (wt%) weight in this region due to thermal decomposition, the RF samples remains 88.4 (wt%) weight, finally.

**Table 4.13** The weight loss (wt%) and stability temperature of AC and RF PPEDOT thin films.

Region	Temperature range (K)	Weight loss (wt %) of PPEDOT (AC) thin films	
		AC (37 W)	RF (37 W)
A	298 – 350	0.51	1.23
B	350- 460	1.47	1.41
C	460-785	7.51	8.72
Stability temperature (K)		592	630

The evolution of low molecular weight hydrocarbon molecules may have caused the reaction. The DSC thermogram reveals exothermic wide band that peaks about 592 K and 630 K for AC and RF samples, respectively. It suggests that the rate of mass loss is increasing. As a result, PPEDOT (RF) films are thermally stable up to around 630 K.

So, the AC plasma polymerized thin film is thermally stable up to about 592K, but the RF plasma polymerized thin film is thermally stable up to about 630 K, however breakdown is delayed for the PPEDOT (RF) thin films, as shown in Fig. 4.26 (b).

#### 4.7.6 DC Electrical Properties: *J-V* Characteristics

To explain the DC electrical conduction mechanism in PPEDOT (RF) thin films, dependence of *J* has been observed on PPEDOT (RF) thin films of various thicknesses in the voltage range of 0.3 to 100 V at different temperatures. The observed *J-V*

characteristics of the AC and RF PPEDOT films at various temperatures are presented in Fig. 4.27.

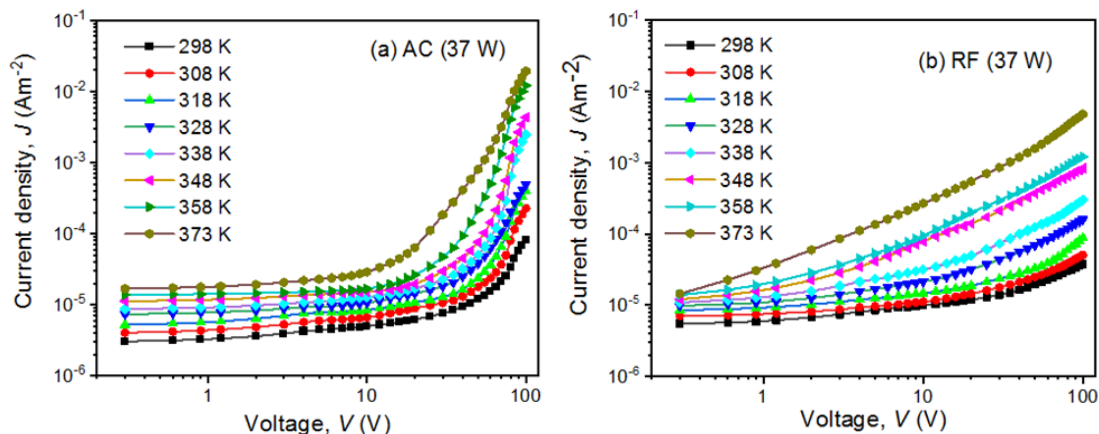


**Fig. 4.27** Current density ( $J$ ) - Voltage ( $V$ ) relationship at different temperatures for (a) PPEDOT (AC) and (b) PPEDOT (RF) films deposit at same power (37 W).

Like those of PPEDOT (AC) films each  $J$ - $V$  curve of the PPEDOT (RF) films also demonstrates different slopes in the lower and higher voltage regions, which indicate two different conduction processes one also operative in this film according to the power law with different values of  $n$ , which are presented in Table 4.14.

**Table 4.14** The slopes in the lower and higher voltage regions at different temperature for PPEDOT thin films of different power sources.

Temperature, $T$ (K)	Value of slopes, $n$			
	Low voltage region ( $<15\text{V}$ ) (Ohmic)		High voltage region ( $> 15\text{V}$ ) (non-Ohmic)	
	AC	RF	AC	RF
298	0.17	0.18	1.03	0.61
308	0.18	0.17	1.11	0.84
318	0.17	0.13	2.73	0.87
328	0.19	0.23	2.33	1.01
338	0.14	0.31	2.98	1.17
348	0.17	0.66	3.03	1.03
358	0.21	0.71	3.12	1.11
373	0.13	0.84	3.15	1.27

At the lower voltage region ( $<15$  V), the values of slope  $0.13 \leq n \leq 0.84$  for RF samples indicate approximate Ohmic region while at the higher voltage region ( $>15$  V), the slopes of  $0.61 \leq n \leq 1.27$  represent the non-Ohmic region.

Again, the values of  $n$  in AC samples lies in between  $0.13 \leq n \leq 0.21$  indicating Ohmic conduction mechanism whereas in the high voltage region ( $>15$  V), the slope of the graph is found to lie in 1.03 - 3.15, indicating a non-Ohmic conduction mechanism.

#### 4.7.7 Dependence of $J$ on temperature

The variation of  $J$  with inverse absolute temperature  $1/T$  for the AC and RF PPEDOT thin films of different power sources are presented in Fig. 4.28. The activation energies calculated from the slope of  $J$  vs  $1/T$  curves and the values are set out in Table 4.15.

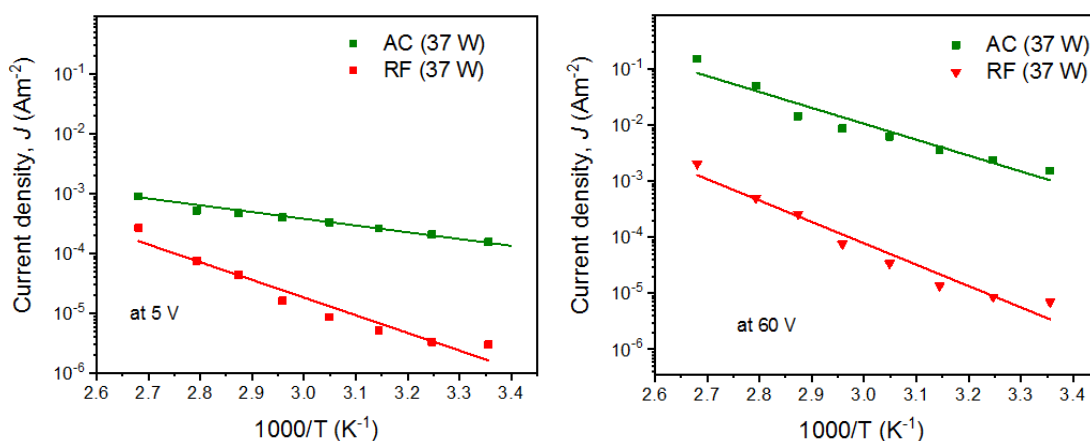


**Fig. 4.28** Comparison of  $J$  on  $1/T$  for PPEDOT (AC) and, PPEDOT (RF) thin films at (a) 5 V (Ohmic) and (b) 60 V (non-Ohmic) regions.

**Table 4.15** Values of activation energy  $\Delta E$  (eV) for PPEDOT (AC) and PPEDOT (RF) thin films.

PPEDOT	Activation energies, $\Delta E$ (eV)	
	5 V (Ohmic)	60 V (non-Ohmic)
AC (37 W)	0.066	0.108
RF (37 W)	0.096	0.125

The activation energy in Ohmic and non-Ohmic regions for PPEDOT (RF) is greater than that of PPEDOT (AC) for applied voltage 5 V and 60 V as shown in Table 4.15. The low and high values of activation energy in Ohmic and non-Ohmic region indicate the transition of carriers between defects within the band gaps and the transition



of carriers between the bands, respectively [66]. In the low temperature regions about an applied voltage of 5 V, the activation energies are found to be around 0.066 eV for AC samples and 0.096 eV for RF samples but in the higher temperature region it has increased up to 0.125 eV. Low activation energy in the low temperature region implies that these films use thermally induced hopping conduction. The changes in activation energy from lower to higher values in high temperature regions might be connected to a transition from hopping to a regime with separate energy levels [66].

In Table 4.16, several properties of AC and RF plasma polymerized thin films such as morphological, structural, optical, and conduction mechanisms acquired from various experimental investigations are recorded.

**Table 4.16** Morphological, structural, thermal, optical and DC electrical properties of as-deposited AC and RF PPEDOT thin films.

Property	AC (37 W)	RF (37 W)
Film thickness	250 nm	660 nm
Surface morphology	Smooth and pinhole free	Smooth and pinhole free
Elemental constituent	Pure	Pure
Functional group	Some new bands created	Some broad and strong bands created
Band gap energy	3.75 eV	3.77 eV
Urbach energy	0.78 eV	0.88 eV
Steepness parameter	0.033	0.029
Refractive index	2.64	2.61
Thermal stability	Stable up to 592 K	Stable up to 630 K
Activation energy	0.076 eV in Ohmic, and 0.119 eV in non-Ohmic region	0.096 eV in Ohmic, and 0.125 eV in non-Ohmic region

It is noticeable from this comparative study that RF power source can produce thicker films within shorter time compared to AC power source, but no significant changes are found in the film's quality in terms of structural, optical, and electrical properties. Again, thickness is the most significant parameters in thin film technology where the films containing low thickness have more applications because of its light weight and interesting physio-chemical properties. In this study, thickness of RF films has showed greater value compared to AC films, so RF is not better than AC PPEDOT films.

## CHAPTER 5

### SUMMARY AND CONCLUSIONS

#### 5.1 Summary

A capacitively coupled parallel plate glow discharge plasma reactor was used to fabricate PPEDOT by thin films onto glass substrates AC and RF. Several characterizations such as FESEM, FTIR, UV-Vis spectroscopy, TG/DSC and DC electrical measurements were carried out to investigate the morphological, structural, optical, thermal and DC electrical properties of the PPEDOT thin films of different thicknesses and power sources.

Surface morphological and topographical studies of the AC PPEDOT thin films were carried out by FESEM analyses. All the films are found smooth, flawless, and pin-hole free. The EDX analysis indicates the presence of prominent percentage of C, S, and a few percentages of O in the PPEDOT thin films, which confirm the elemental purity of PPEDOT thin films.

To understand the chemical structure and optical properties of the films, the FTIR and UV-Vis spectroscopic analyses are used, respectively. As compared to the monomer spectrum, the intensity of absorbing bands has decreased significantly, and a few new peaks are found in the AC plasma spectra, which are not present in the monomer spectrum. These are the indication of degradation or re-organization of the monomer molecules during the plasma polymerization process.

Absorbance of PPEDOT (AC) thin films has increased with increasing film thicknesses and peak values are placed in lower wavelength region due to the presence of the  $\pi$ - $\pi$  conjugation or it may happen an increase in scattering with increasing thickness. Around 86% transmittance at  $\sim 575 - 735$  nm wavelengths is recorded that confirmed transparency of all the films in the visible region. The absorption changes with photon energy following an exponential fall in the low energy region, which is caused by the lack of long-range order films or existence of defects. The optical band gap value decreases from 3.75 to 3.54 eV with increasing thickness of the films due to some crosslinking may occurring inside the bulk of the material because of the influence of plasma on the surface during the deposition process. The calculated Urbach energy

values have decreased from 0.78 to 0.56 eV with increasing film thickness which indicate less structural disorder in the introduction of localized states within the forbidden energy bandgap. The extinction coefficient has increased suggesting that electron transports across the mobility gap with wavelength. The refractive index values for all samples have reached to 2.64 corresponding 400 nm wavelength region which indicates the increase in interactions taking place between the photons and electrons of the films. The optical conductivity value of the samples approach zero at higher wavelengths (above 600 nm) for all the deposited PPEDOT thin films. The skin depth has fallen monotonically with increasing photon energy and broadened with diverse film power sources because of increased electron collisions causing energy loss.

The thermal analyses of PPEDOT thin films in N<sub>2</sub> environment reveal that PPEDOT (AC) thin films are thermally stable up to 590 to 612 K temperature after losing about 10 to 12% weight. Maximum weight loss has occurred due to thermal decomposition of the PPEDOT samples.

In the lower voltage region, *J-V* characteristics revealed that the dependence of current density is Ohmic and in higher voltage region it is non-Ohmic. It is found from *J-d* graph that the dominant conduction mechanism in the PPEDOT thin films is SCLC type. The activation energy,  $\Delta E$ , values of the PPEDOT thin films in the Ohmic region (10 V) are found to be around an average value of 0.076 eV whereas in the non-Ohmic region (60 V),  $\Delta E$  were found to be around 0.119 eV.

The comparison study of SEM reveals that surfaces of both films are smooth and pin-hole free. The EDX analysis indicates the elemental purity of these thin films and structural changes between AC and RF films is occurred due to different power sources. The values of energy band gap for the PPEDOT (RF) thin film is slightly higher (~ 3.77 eV) compared to PPEDOT (AC) thin film. PPEDOT (RF) films are more thermally stable than PPEDOT (AC) up to about 630 K. The weight loss for RF PPEDOT thin film is greater than that of the AC PPEDOT thin film. Thus, it can be inferred that though RF plasma polymerized thin films are more stable as compared to the AC plasma polymerized thin film, however, their degradation is delayed for RF plasma films.

It can be summarized that both AC and RF PPEDOT thin films have showed almost similar properties, but difference of thickness is comparatively so high. In AC PPEDOT films, with increasing film thickness (from 250 to 390 nm) band gap is decreased from 3.75 to 3.54 eV whereas the band gap of RF sample (690 nm thickness) is 3.77 eV. RF generator has produced the films whose thickness including band gap is higher than AC plasma. After all, it can be summarized that RF is not so good as AC PPEDOT films.

## 5.2 Conclusions

It is concluded that high quality of PPEDOT thin films have been successfully deposited on to glass substrates by plasma polymerization technique. Plasma polymerization can produce PPEDOT thin films of better surface morphology containing with elemental purity.

FTIR analysis confirms that the chemical structures of the deposited films are changed during the polymerization, indicating a defragmentation of the monomer and the structure of PPEDOT departs from that of the monomer structure.

Absorbance and transmittance analyses confirmed that all the films exhibit improved transport performance in the visible region which are suitable to be applied in high performance photovoltaic devices. The Urbach energy suggests the better introduction of localized states within the forbidden energy bandgap and the refractive index indicates the increase in interactions taking place between the photons and electrons of the films. The obtained extinction coefficient values indicate the probability of electron transfer across the mobility gap rises with photon energy.

The TG/DSC thermogram reveals the weight loss and exothermic wide band of AC and RF samples, which indicates that these films are very thermally stable up to about 630 K. The dominant conduction mechanism in the PPEDOT films exhibited SCLC mechanism.

From comparative study of AC and RF PPEDOT thin films, AC power source is more effective to produce polymer thin film.

Finally, the PPEDOT thin films were found to be physically, chemically, and optically stable. The outcomes of the fundamental characterizations of PPEDOT thin films

suggest that the films have great potential for organo-electronic, photovoltaic, and thermoelectric applications.

### **5.3 Scope of the Further Research**

In this present work, various characterizations such as morphological, structural, thermal, optical and DC electrical properties of as-deposited AC and RF PPEDOT thin films are performed. Apart from this, some additional characterizations can be carried out in order to get better understand the suitability of PPEDOT thin films for different applications.

- Thickness dependent RF samples can be prepared to investigate further study of the PPEDOT thin films.
- AC electrical properties of the PPEDOT thin films can be done to better understand the electrical and dielectric properties of the material.
- Annealing effect on the PPEDOT thin films can be studied to understand the properties of the films more clearly.

## References

- [1] Galli, P., Vecellio, G., “Technology: driving force behind innovation and growth of polyolefins,” *Prog. Polym Sci.*, Vol. 26 (8), pp. 1287-336, 2001.
- [2] Barber, P., Balasubramanian, S., Anguchamy, Y., Gong, S., Wibowo, A., Gao, H., Ploehn, H.J., and Zur Loye, H.C., “Polymer composite and nanocomposite dielectric materials for pulse power energy storage,” *Mater.*, Vol. 2(4), pp. 1697-1733, 2009.
- [3] Radeva, E., Georgieva, V., Lazarov, J., Gadjanova, V., Tsankov, D., “Plasma polymerized hexamethyldisiloxane thin films for NO<sub>2</sub> gas sensor application,” *Dig. J. Nanomater. Biostructures*, Vol. 9, pp. 459-466, 2014.
- [4] Guermat, N., Bellel, A., Sahli, S., Segui, Y., and Raynaud, P., “Plasma polymerization of hexamethyldisiloxane and tetraethoxysilane thin films for humidity sensing application,” *Defect Diffus. Forum.*, Vol. 354, pp. 41-47, Trans Tech Publications Ltd, 2014.
- [5] Farahani, H., Wagiran, R., Hamidon, M.N., “Humidity sensors principle, mechanism, and fabrication technologies: a comprehensive review,” *Sensors*, Vol. 14, pp. 7881-7939, 2014.
- [6] Gomathi, N., Sureshkumar, Sudarsan, N., “RF plasma-treated polymers for biomedical application,” *Curr. Sci.*, Vol. 94, pp. 1478-1486, 2008.
- [7] Aviraj, A.J., Jyotiprakash, B.Y., Deshmukh, R.R., Harish, C.B., Vijaya, P., Puri, R.K., “Glow discharge plasma polymerized nanostructured polyaniline thin film optical waveguide,” *Adv. Mater. Lett.*, Vol. 8, pp. 180-184, 2017.
- [8] Sheats, J.R., Antoniadis, H., Hueschen, M., Leonard, W., Miller, J., Moon, R., Roitman, D. and Stocking, A., “Organic electroluminescent devices,” *Sci.*, Vol. 273(5277), pp. 884-888, 1996.
- [9] Olivares, A.J., Cosme, I., Sanchez-Vergara, M.E., Mansurova, S., Carrillo, J.C., Martinez, H.E., and Itzmoyotl, A., “Nanostructural modification of PEDOT: PSS for high charge carrier collection in hybrid frontal interface of solar cells,” *Polym.*, Vol. 11(6), pp. 1034, 2019.
- [10] Na, J.Y., Kang, B., Sin, D.H., Cho, K., and Park, Y.D., “Understanding solidification of polythiophene thin films during spin-coating: effects of spin-coating time and processing additives,” *Sci. Rep.*, Vol. 5(1), pp. 1-14, 2015.

- [11] Ziaee, A., O'Dea, S., Howard-Hildige, A., Padrela, L., Potter, C., Iqbal, J., Albadarin, A.B., Walker, G., and O'Reilly, E.J., "Amorphous solid dispersion of ibuprofen: A comparative study on the effect of solution-based techniques," *Int. J. Pharm. Res.*, Vol. 572, pp. 118816, 2019.
- [12] Oskam, G., Long, J.G., Natarajan, A., and Searson, P.C., "Electrochemical deposition of metals onto silicon," *J. Phy.*, Vol. 31(16), pp. 1927, 1998.
- [13] Cho, Seung Il, Rui Xiao, and Sang Bok Lee, "Electrochemical synthesis of poly (3,4-ethylenedioxythiophene) nanotubes towards fast window-type electrochromic devices," *J. Nanotechnol.*, Vol. 18(40), pp. 405705, 2007.
- [14] Kong, L.B., Zhang, J., An, J.J., Luo, Y.C., and Kang, L., "MWNTs/PANI composite materials prepared by in-situ chemical oxidative polymerization for supercapacitor electrode," *J. Mater. Sci.*, Vol. 43(10), pp. 3664-3669, 2008.
- [15] Massines, F., Gherardi, N., Fornelli, A., and Martin, S., "Atmospheric pressure plasma deposition of thin films by Townsend dielectric barrier discharge," *Surf. Coat. Technol.* Vol. 200(5-6), pp. 1855-1861, 2005.
- [16] Liang, L., Shi, M., Viswanathan, V.V., Peurrung, L.M., and Young, J.S., "Temperature-sensitive polypropylene membranes prepared by plasma polymerization," *J. Membr. Sci.*, Vol. 177(1-2), pp. 97-108, 2000.
- [17] Guerin, D.C., Hinshelwood, D.D., Monolache, S., Denes, F.S. and Shamamian, V.A., "Plasma polymerization of thin films: Correlations between plasma chemistry and thin film character," *Langmuir*, Vol. 18(10), pp. 4118-4123, 2002.
- [18] Friedrich, J., "Mechanisms of plasma polymerization-reviewed from a chemical point of view," *Plasma Process Polym.*, Vol. 8(9), pp. 783-802, 2011.
- [19] Jiang, H., Hong, L.G., Venkatasubramanian, N., Grant, J.T., Eyink, K., Wiacek, K., Fries-Carr S., Enlow, J., Bunning, T.J., "The relationship between chemical structure and dielectric properties of plasma-enhanced chemical vapor deposited polymer thin films," *Thin Solid Films*, Vol. 515, pp. 3513-3520, 2007.
- [20] Lakshmi, G.B. V.S., Dhillon, A., Avasthi, D.K., Siddiqui, A., "Synthesis and characterization of thin films of poly (3-methyl thiophene) by RF-plasma polymerization," *Mater. Lett.*, Vol. 64(15), pp. 1672-1673, 2010.
- [21] Kiristi, M., Bozduman, F., Oksuz, A.U., Hala, A., and Oksuz, L., "A comparison study of microwave and radio frequency plasma polymerized PEDOT thin films," *J. Macromol. Sci. Part A*, Vol. 52(2), pp. 124-129, 2015.

- [22] Jiang, H., Hong, L., Venkatasubramanian, N., Grant, J.T., Eyink, K., Wiacek, K., and Bunning, T.J., "The relationship between chemical structure and dielectric properties of plasma-enhanced chemical vapor deposited polymer thin films," *Thin Solid Films*, Vol. 515(7-8), pp. 3513-3520, 2007.
- [23] Pachonik, H., "Production of thin glow-polymerized layers," *Thin Solid Films*, Vol. 38, pp. 171-182, 1976.
- [24] Tibbit, J.M., Bell, A.T., and Shen, M., "Dielectric relaxations in plasma polymerized hydrocarbons and fluorocarbons," *J. Macromol. Sci.-Chem. A*, Vol. 10, pp. 519-533, 1976.
- [25] Yasuda, H., "Glow discharge polymerization," *Thin Film Processes 1*, 361, 1978.
- [26] Lin, C.L., Chen, C.Y., Yu, H.F., and Ho, K.C., "Comparisons of the electrochromic properties of poly (hydroxymethyl 3,4-ethylenedioxythiophene) and poly (3,4-ethylenedioxythiophene) thin films and the photoelectrochromic devices using these thin films," *Sol. Energy Mater Sol. Cells*, Vol. 202, pp. 110132, 2019.
- [27] Kabir, H., Rahman, M.M., Roy, T.S., and Bhuiyan, A.H., "Structural and optical properties of plasma polymerized pyromucic aldehyde thin films," *Int. J. Mech. Mechatron. Eng.*, Vol. 12, pp. 30-34, 2012.
- [28] Karaca, G.Y., Eren, E., Alver, C., Koc, U., Uygun, E., Oksuz, L., and Oksuz, A.U., "Plasma modified V<sub>2</sub>O<sub>5</sub>/PEDOT hybrid based flexible electrochromic devices," *Electroanalysis*, Vol. 29(5), pp. 1324-1331, 2017.
- [29] Kiristi, M., Bozduman, F., Oksuz, A.U., Hala, A., and Oksuz, L., "A comparison study of microwave and radio frequency plasma polymerized PEDOT thin films," *J. Macromol. Sci. A*, Vol. 52(2), pp. 124-129, 2015.
- [30] Chang, S.H., Chiang, C.H., Kao, F.S., Tien, C.L. and Wu, C.G., "Unraveling the enhanced electrical conductivity of PEDOT: PSS thin films for ITO-free organic photovoltaics," *IEEE Photonics J.*, Vol. 6(4), pp. 1-7, 2014.
- [31] Ramdzan, N.S. M., Fen, Y.W., Liew, J.Y.C., Omar, N.A.S., Anas, N.A.A., Daniyal, W.M.E. M.M., and Fauzi, N.I.M., "Exploration on structural and optical properties of nanocrystalline cellulose/poly (3,4-ethylenedioxythiophene) thin film for potential plasmonic sensing application," *Photonics*, Vol. 8(10), Multidisciplinary Digital Publishing Institute, 2021.



- [32] Nasrin, R., Rahman, M.J., Jamil, A.T.M.K., Hossain, K.S., and Bhuiyan, A.H. "Thickness dependent structural and surface properties of plasma polymerized N-benzylaniline thin films," *Appl. Phys. A*, Vol. 127(4), pp. 1-12, 2021.
- [33] Sarker, R.B. and Bhuiyan, A.H., "Electrical conduction mechanism in plasma polymerized 1-benzyl-2-methylimidazole thin films under static electric field," *Thin Solid Films*, Vol. 519, pp. 5912-5916, 2011.
- [34] Manaa, C., Bouaziz, L., Lejeune, M., Kouki, F., Zellama, K., Benlahsen, M., Mejatty, M., and Bouchriha, H., "Detailed investigation of optoelectronic and microstructural properties of plasma polymerized cyclohexane thin films: dependence on the radiofrequency power," *J. Appl. Phys.*, Vol. 117, pp. 215701-215708, 2015.
- [35] Momin, M., Hossain, K.S., and Bhuiyan, A.H., "Microstructural, compositional, topological and optical properties of plasma polymerized cyclohexane amorphous thin films," *J. Polym. Res.*, Vol. 26(3), pp. 1-10, 2019.
- [36] Giuri, A., Masi, S., Colella, S., Listorti, A., Rizzo, A., Kovtun, A., "Rheological and physical characterization of PEDOT: PSS/graphene oxide nanocomposites for perovskite solar cells," *Polym. Eng. Sci.*, Vol. 57(6), pp. 546-552, 2017.
- [37] Shen, M., and Bell, A.T., "A review of recent advances in plasma polymerization," pp. 1-33, 1979.
- [38] Chan, C.M., Ko, T.M., and Hiraoka, H., "Polymer surface modification by plasmas and photons," *Surf. Sci. Rep.*, Vol. 24(1-2), pp. 1-54, 1996.
- [39] Yasuda, H., and Hirotsu, T., "Critical Evaluation of Conditions of Plasma Polymerization," *J. Polym. Sci., Polym. Chem. Ed.*, Vol.16, pp. 313-317, 1978.
- [40] Yasuda, H., and Lamaze, C.E., "Polymerization in an electrode less glow discharge. III. organic compounds without olefinic double bond," *J. Appl. Polym. Sci.*, Vol. 17, pp. 1533-1544, 1973.
- [41] Conrads, H., and M. Schmidt. "Plasma generation and plasma sources," *Plasma Sources Sci. Technol.*, Vol. 9(4), pp. 441, 2000.
- [42] Hoffmann, V., Gijbels, R., and Wetzig, K., "Comparison of modeling calculations with experimental results for RF glow discharge optical emission spectrometry." *Spectrochim. Acta. Part B At. Spectrosc.*, Vol. 57(1), pp. 109-119, 2002.

- [43] Han, S., Feng, Y., Chen, G., and Wang, J., "Facile preparation of composites composed of high-performance thermoplastic and difficult-to-process functional polymer," *RSC Adv.*, Vol. 4(60), pp. 31874-31878, 2014.
- [44] Groenendaal, L., Jonas, F., Freitag, D., Pielartzik, H., and Reynolds, J.R., "Poly (3, 4-ethylenedioxythiophene) and its derivatives: past, present, and future," *Adv. Mater.*, Vol. 12(7), pp. 481-494, 2000.
- [45] Lamb, D.R., "Electrical conduction mechanisms in thin insulating films," Methuen and Co. Ltd., London, 1967.
- [46] Bhattacharyya, S., Laha, A., and Krupanidhi, S.B., "Analysis of leakage current conduction phenomenon in thin  $\text{SrBi}_2\text{Ta}_2\text{O}_9$  films grown by excimer laser ablation," *J. Appl. Phys.*, Vol. 91, pp. 4543-4548, 2002.
- [47] Anderson, L.J., and Jacob, M.V., "Electrical characterisations of plasma polymerised linalyl acetate," *Mater. Sci. Eng. B*, Vol. 177, pp. 311-315, 2012.
- [48] Simmons, J.G., "Poole-Frenkel effect and Schottky effect in metal-insulator-metal systems," *Phys. Rev. Appl.*, Vol. 115, pp. 657-660, 1967.
- [49] Gould, R.D., "The interpretation of space-charge-limited currents in semiconductors and insulators," *J. Appl. Phys.*, Vol. 53, pp. 3353-3355, 1982.
- [50] Silverstein, M.S., and Visoy, F.I., "Plasma polymerized thiophene: molecular structure and electrical properties," *Polym.*, Vol. 43, pp.11-20, 2002.
- [51] Matin, R., and Bhuniyan, A.H., "Electrical transport mechanism in plasma polymerized 2, 6, diethylaniline thin films," *Thin Solid Films*, Vol. 519, pp. 3462-3467, 2011.
- [52] Yang, J., Lee, S., Park, H., and Jung, D., "Characterization of low dielectric constant plasma polymer films deposited by plasma-enhanced chemical vapor deposition using decamethylcyclopentasiloxane and cyclohexane as the precursors," *J. Vac. Sci. Technol. A.*, Vol. 24, pp. 165-169, 2006.
- [53] Kabir, H., Nasrin, R., Rahman, M.M., and Bhuiyan, A.H., "Heat treatment effect on the structural, morphological, and optical properties of plasma polymerized furan-2-carbaldehyde thin films," *Results Phys.*, pp. 103014, 2020.
- [54] Khan, S., Majid, A., and Raza, R., "Synthesis of PEDOT: PPy/AC composite as an electrode for supercapacitor," *J. Mater. Sci.: Mater. Electron.*, Vol. 31, pp 13597-13609, 2020.

- [55] Zarrin, N., Tavanai, H., Abdolmaleki, A., Bazarganipour, M., "An investigation on the fabrication of conductive polyethylene dioxythiophene (PEDOT) nanofibers through electrospinning," *Synth. Met.*, Vol. 244, pp. 143-149, 2018.
- [56] Yewale, R., Damlin, P., Salomaki, M., and Kvarnstrom, C., "Layer-by-layer approach to engineer and control conductivity of atmospheric pressure vapor phase polymerized PEDOT thin films," *Mater. Today Commun.*, Vol. 25, pp. 101398, 2020.
- [57] Banwell, C.N., and Mc Cash, E.M., "Fundamentals of molecular spectroscopy," *McGraw-Hill*, London, 1994.
- [58] Rahman, M.J., and Bhuiyan, A.H., "Structural and optical properties of plasma polymerized o-methoxyaniline thin films," *Thin Solid Films*, Vol. 534, pp. 132-136, 2013.
- [59] Bae, I.S., Jung, C.K., Cho, S.J., Song, Y.H., and Boo, J.H., "A comparative study of plasma polymerized organic thin films on their electrical and optical properties," *J. Alloys Compd.*, Vol. 449(1-2), pp. 393-396, 2008.
- [60] Chowdhury, F.U.Z., and Bhuiyan, A.H., "An investigation of the optical properties of plasma-polymerized diphenyl thin films," *Thin Solid Films*, Vol. 360(1-2), pp. 69-74, 2000.
- [61] Baco, S., Chik, A. and Yassin, F.M., "Study on optical properties of tin oxide thin film at different annealing temperature," *J. Sci. Tech.*, Vol. 4(1), 2012.
- [62] Tauc, J., Menth, A., and Wood, D.L., "Optical and magnetic investigations of the localized states in semiconducting glasses," *Phys. Rev. Lett.*, Vol. 25(11), pp. 749, 1970.
- [63] Anderson, L.J., and Jacob, M.V., "Electrical characterisations of plasma polymerised linalyl acetate," *Mater. Sci. Eng. B*, Vol. 177(3), pp. 311-315, 2012.
- [64] Dakhel, A. A., "Mechanisms of DC-current transfer in tris (acetylacetonato) iron (III) films," *J. Non-Cryst. Solids*, Vol. 353(16-17), pp. 1529-1533, 2007.
- [65] Matin, R., and Bhuiyan, A.H., "Electrical transport mechanism in plasma polymerized 2, 6, diethylaniline thin films," *Thin Solid Films*, Vol. 519(11), pp. 3462-3467, 2011.
- [66] Gould, R.D., "The interpretation of space-charge-limited currents in semiconductors and insulators," *J. Appl. Phys.*, Vol. 53, pp. 3353-3355, 1982.

**List of Presentations:**

1. Md. Juel Sarder, Mohammad Jellur Rahman, Md. Mahmud Hasan, and A. H. Bhuiyan, “Comparative study of power and thickness dependent optical properties of ac plasma polymerized 3,4-ethylenedioxythiophene thin films obtained by AC plasma polymerization technique,” organized by Bangladesh Physical Society, Dhaka, Bangladesh, 06-07 August 2021. (Selected as the best oral presentation).
2. Md. Juel Sarder, Mohammad Jellur Rahman, Md. Mahmud Hasan, and A. H. Bhuiyan, “Thickness dependent optical properties of the AC plasma polymerized 3,4-ethylenedioxythiophene thin films,” International e-Conference on Physics, organized by the department of Physics, University of Dhaka, 9-11 July 2021.



## **NATIONAL CONFERENCE ON PHYSICS-2021**

**06 – 07 August 2021**

**Theme  
PHYSICS FOR NATIONAL DEVELOPMENT**

### **PROGRAMME & ABSTRACTS**

**Venue  
Zoom Online Platform**



**Organized by  
Bangladesh Physical Society**

**TF-02: Comparative study of power and thickness dependent optical properties of AC plasma polymerized 3,4-Ethylenedioxythiophene thin films**

**Md. JuelSarder<sup>a</sup>, Mohammad Jellur Rahman<sup>a</sup>, Md. Mahmud Hasan<sup>a</sup>, and A. H. Bhuiyan<sup>a,b</sup>**

<sup>a</sup>Department of Physics, Bangladesh University of Engineering and Technology, Dhaka-1000, Bangladesh

<sup>b</sup>University of Information Technology and Sciences, Baridhara, Dhaka-1212, Bangladesh

\*Email: mjrahman@phy.buet.ac.bd

Organic polymer thin films have attained significant research attention in the last few decades. Plasma polymerization is a distinctive technique for direct polymeric thin films deposition from different organic monomers. The organic compound 3,4-ethylenedioxythiophene (EDOT) has been chosen as monomer to deposit plasma polymerized EDOT (PPEDOT) thin films. The polymerization is carried out by using a capacitively coupled glow discharge reactor by optimizing the plasma parameters, where the plasma is created at line frequency (50 Hz). Thicknesses of the thin films are varied by synthesizing PPEDOT thin films for different deposition times and input powers. Optical parameters of the deposited PPEDOT thin films such as the absorbance, absorption coefficient, optical band gap energies, Urbach energy, extinction coefficient, refractive index, etc. are obtained from UV-visible spectra and are correlated to understand their applicability. From the UV-Vis analysis, it is observed that the values of direct band gap energy,  $E_{g(d)}$ , varies from 3.94 to 3.86 eV and that of the indirect band gap energy,  $E_{g(i)}$ , varies from 3.62 to 3.20 eV for the PPEDOT thin films of different thicknesses. The decrease of  $E_{g(d)}$  and  $E_{g(i)}$  values with the increasing thicknesses is due to the increase in fragmentation/cross-linking in the bulk of the material due to the impact of plasma on the surface of the thin films during polymerization. The values of the Urbach

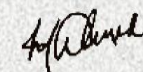


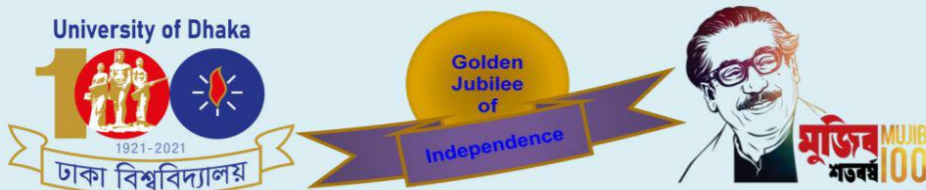
National Conference on Physics - 2021  
06- 07 August, 2021  
Organized by: Bangladesh Physical Society

**Best Presentation Certificate**

This is to certify that the Presentation TF-02: Comparative study of power and thickness dependent optical properties of AC plasma polymerized 3,4-Ethylenedioxythiophene thin films: by Md. Juel Sarder, Mohammed Jellur Rahman, Md. Mahmud Hasan, and A. H. Bhuiyan has been selected as the best Oral Presentation in the National Conference on Physics - 2021 organized by Bangladesh Physical Society, held through Virtual Platform during 06- 07 August, 2021.

  
Dr. Mohammed Nazrul Islam Khan  
General Secretary

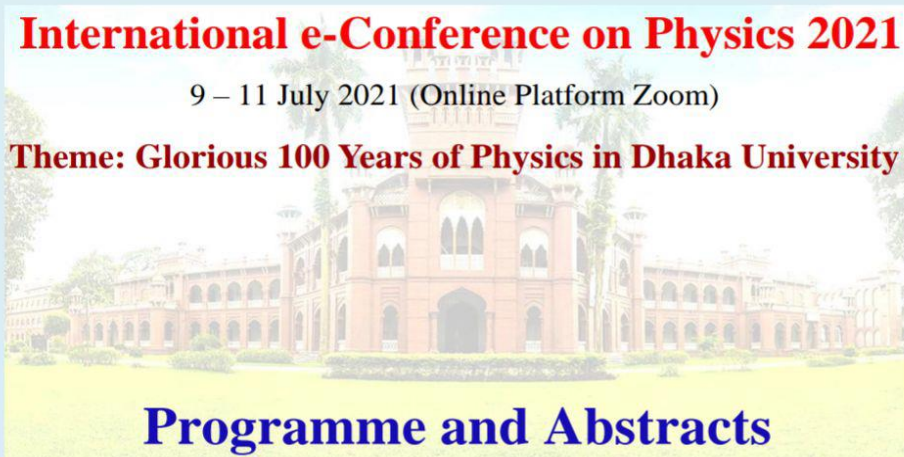
  
Prof. Dr. Mesbahuddin Ahmed  
President



## **International e-Conference on Physics 2021**

9 – 11 July 2021 (Online Platform Zoom)

**Theme: Glorious 100 Years of Physics in Dhaka University**



## **Programme and Abstracts**



Organized

by

Department of Physics

University of Dhaka

## ECMP-06: Thickness Dependent Optical Properties of the AC Plasma Polymerized 3,4-Ethylenedioxythiophene Thin Films

Md. Juel Sarder<sup>1</sup>, Mohammad Jellur Rahman<sup>1,\*</sup>, Md. Mahmud Hasan<sup>1</sup>, and A. H. Bhuiyan<sup>1,2</sup>

<sup>1</sup>Department of Physics, Bangladesh University of Engineering and Technology, Dhaka-1000, Bangladesh

<sup>2</sup>University of Information Technology and Sciences, Baridhara, Dhaka-1212, Bangladesh

\*Email: mjrahman@phy.buet.ac.bd

Plasma polymerization is a distinctive technique for direct polymeric thin films deposition from different organic monomers. The organic compound 3,4-ethylenedioxythiophene (EDOT) has been chosen as monomer to deposit plasma polymerized EDOT (PPEDOT) thin films. The polymerization is carried out by using a capacitively coupled glow discharge reactor by optimizing the plasma parameters, where the plasma is created at line frequency (50 Hz). Thicknesses of the thin films are varied by synthesizing PPEDOT thin films for different deposition times and powers, where the thicknesses are measured by Multiple-Beam interferometer technique. Different optical parameters such as the absorbance, absorption coefficient, direct and indirect band gap energies, Urbach energy, extinction coefficient, refractive index, optical conductivity, skin depth are obtained from UV-visible spectra of the deposited PPEDOT thin films and are correlated to understand the applicability of the PPEDOT thin films. From the UV-Vis analysis, it is observed that the values of direct band gap energy,  $E_{g(d)}$ , varies from 3.94 to 3.86 eV and that of the indirect band gap energy,  $E_{g(i)}$ , varies from 3.62 to 3.20 eV for the PPEDOT thin films of different thicknesses. The decrease of  $E_{g(d)}$  and  $E_{g(i)}$  values with the increasing thicknesses is due to the increase in fragmentation/cross-linking in the bulk of the material due to the impact of plasma on the surface of the thin films with plasma duration. The values of the Urbach energy,  $E_u$  varies from 0.00364 to 0.00258 eV with the variation of thickness due to the increase of disorder in the PPEDOT thin films.